# STIFFNESS AND DAMPING EVALUATION OF AIR BEARING SLIDERS BY MODAL ANALYSIS METHODS: NEW DESIGNS WITH HIGH DAMPING

**Q. H. Zeng[1] and D. B. Bogy**
Computer Mechanics Laboratory
Department of Mechanical Engineering
University of California
Berkeley, CA 94720

## ABSTRACT

The dynamic characteristics of slider-air bearings in hard disk drives is an important issue for the drive's performance. We apply the dynamic simulation and modal analysis method to analyze the dynamic properties of slider-air bearings. First, the theoretical background is briefly described. A procedure for modal parameter estimation is proposed, and an iteration method is established to obtain the stiffness and damping matrices of the bearings. Then, five typical designs, one of which is first proposed in this report, of the air bearing surfaces (ABS) are briefly discussed. The dynamic properties and effects of speed and skew angle are investigated. The dynamic characteristics of the five designs are compared. It is found that a negative pressure slider has the highest stiffness and lowest damping, the TPC and two newly proposed sliders demonstrate higher damping. Finally, the complicated ABS design problem is briefly discussed. A slider is designed, analyzed and compared with other sliders. The air bearing of the new slider design has larger stiffness and the highest damping of those studied. The results indicate that the proposed methods give a theoretically sound and rational means for determining stiffness and damping of air bearing sliders, and that the approach presented in this report should be useful for high performance slider design.

[1] Visiting researcher, Associate professor, Institute of Vibration Engineering, Nanjing University of Aeronautics & Astronautics, Nanjing, China.

## 1. Introduction

Dynamic characteristics of slider-air bearings is an important issue for lower and more stable flying heights, faster slider settling, and more reliable slider-disk interfaces to further improve the performance of hard disk drives. Especially, as flying heights continue to decrease, the intermittent contact and impact of the slider and disk's asperites in the normal operation state are unavoidable. It is then essential for the slider's fluctuation induced by the impacts to be rapidly damped out so that the successive impacts will not drive the slider motion into resonance and result in a crash. Therefore, a better understanding of the dynamic properties, such as stiffness and damping, of the air-bearings becomes an important concern, and high damping properties become one of important design objectives of slider-air bearings.

Analyzing the dynamic characteristics requires solving simultaneously the generalized Reynolds equation and the equation of motion of the slider-suspension assembly. Perturbation methods [1,2,3] have been previously used to obtain approximate solutions. Numerical simulations, such as that provided by the CML Dynamic Simulator[4], have become a powerful tool for the study of the characteristics and the design of slider-disk interfaces. Because the simulations can solve very complicated configurations, and can obtain the dynamic performance information that is required for the design, they are becoming more widely used in industry. Recently, the modal analysis method [5] was used to analyze the dynamic properties of slider-air bearings, and the method was shown to be a versatile tool for head-medium interface analysis. Therefore, in this report, we applied the CML Dynamic Simulator with the modal analysis method to evaluate the dynamic characteristics of several typical ABS designs. The multiple input/multiple output orthogonal rational fractional polynomial method was employed to estimate the modal

parameters of the system, and an iteration procedure was proposed for estimating the stiffness and damping matrices of the air bearing-slider systems.

Many types of air bearing surfaces (ABS) have been designed in past decades. The taper-flat slider (TF) was originally designed for the IBM 3370. It is one of the simplest air-bearing surface designs, and it was widely used in the industry for about 15 years. To achieve preferred performances, such as constant flying height from the inner diameter (ID) to the outer diameter (OD), altitude insensitivity, faster take-off, and lower manufacture tolerance sensitivity, several modified designs have been proposed. For example, there are negative pressure sliders (TFN) [6, 7, 8], transverse pressure contour sliders(TFS), named as "TPC" [9], shaped rail sliders with two or three rails (TFB) [10, 11]. Combining these typical designs, engineers have proposed more complicated designs, such as the Headway AAB design (combined TFN and TFB), the Seagate AAB design [12] (combined TFN, TFB and TFS), and the TNP design [13] (combined TFS and TFN). There are several papers presenting their steady flying properties and some dynamic characteristics. However, their damping properties have not been significantly investigated. Some papers, such as [9, 13, 14, 15] have only presented qualitative damping results. Many papers, such as [16], researched vibration properties, but they gave improper identification of the vibration modes. For example, parallel (or vertical) and pitch modes were defined. In fact, these modes do not exist in most slider-air bearings.

In this report, we present quantitative results for the stiffness, damping and mode shapes of typical slider designs, and then we propose a new design with high damping. The dynamic properties of the chosen designs are compared. The research presented here was focused on comparing the modal frequencies and damping ratios of the designs for three operational speeds and three skew angles. The results show that the different ABS designs have quite different dynamic properties. Finally, the complicated ABS design problem is

briefly discussed, and a slider with a novel ABS is designed, analyzed, and compared with other sliders. It is demonstrated that the newly designed slider generates an air-bearing with relatively high damping.

## 2. Mathematical Background

### 2.1 Governing equations

Figure 1 shows a schematic diagram of the slider geometry and coordinate system. Assuming the slider is a rigid body and vibrates in the range near its steady flying state, we can express the governing equations for the motion of the slider as

$$m\frac{\mathrm{d}^2 z}{\mathrm{d}t^2}+c_z\frac{\mathrm{d}z}{\mathrm{d}t}+k_z z = f_z(t)+\iint_A (p-p_s)\mathrm{d}A \tag{1}$$

$$I_\theta\frac{\mathrm{d}^2\theta}{\mathrm{d}t^2}+c_\theta\frac{\mathrm{d}\theta}{\mathrm{d}t}+k_\theta\theta = f_\theta(t)-\iint_A (p-p_s)x\mathrm{d}A \tag{2}$$

$$I_\beta\frac{\mathrm{d}^2\beta}{\mathrm{d}t^2}+c_\beta\frac{\mathrm{d}\beta}{\mathrm{d}t}+k_\beta\beta = f_\beta(t)+\iint_A (p-p_s)y\mathrm{d}A \tag{3}$$

In Eqs(1)-(3), $z$, $\theta$ and $\beta$ are the slider's vertical displacement (from the steady flying condition) at the slider's center, and its pitch and roll; $m$, $I_\theta$ and $I_\beta$ are the mass and inertia moments of the slider; $k_z$, $k_\theta$, $k_\beta$, $c_z$, $c_\theta$, and $c_\beta$ are stiffness and damping coefficients of the suspension in the three directions. $f_z(t)$, $f_\theta(t)$ and $f_\beta(t)$ are external excitation forces. $p$ and $p_s$ are pressure profiles in the vibration state and steady flying state, governed by the generalized Reynolds equation

$$\frac{\partial}{\partial x}\left(ph^3Q\frac{\partial p}{\partial x}\right)+\frac{\partial}{\partial y}\left(ph^3Q\frac{\partial p}{\partial y}\right)=6\mu V_x\frac{\partial(ph)}{\partial x}+6\mu V_y\frac{\partial(ph)}{\partial y}+12\mu\frac{\partial(ph)}{\partial t}, \tag{4}$$

where $h$ is air bearing thickness; $\mu$ is ambient gas viscosity; $V_x$ and $V_y$ are gas velocity in the x and y directions; $Q$ is a modification function to account for gaseous rarefaction effects. Simultaneously solving the equations, we can obtain the vibration responses for given disturbances, such as impulses, bumps and roughness of the disks. This can be performed by perturbation methods or numerical simulations. Here, we use the system identification method to obtain the system's parameters. For small disturbances to its

steady flying state, assuming the system is linear, time-invariant, self-adjoint, and with viscous damping, we can write Eqs.(1)-(3) as

$$[M]\{\ddot{u}\} + [C]\{\dot{u}\} + [K]\{u\} = \{f(t)\} \tag{5}$$

where [*M*], [*K*] and [*C*] are the mass, stiffness and damping matrices (3x3), and $\{u\}=\{z, \theta, \beta\}^T$ is the vibration displacement vector of the slider.

**2.2 Modal parameters estimation**

First, the steady (or "static") solution is found from Eq.(4) by the Simulator. Next, a small initial velocity $\dot{z}_0$ of the slider in the vertical direction is specified. That is characterized as an impulse force

$$f_z(t) = m\dot{z}_0\delta(t) \tag{6}$$

where δ(t) is Dilac's delta function. The responses of the slider in the three motion directions are calculated by the Simulator, and they are subtracted from the steady solution to obtain the vibration responses *{u(t)}*. Then, the impulse response functions (IRFs) of the system, defined by

$$\{h(t)\} = \frac{\{u(t)\}}{m\dot{z}_0}, \tag{7}$$

are calculated. The Fourier transformations of the IRFs for this disturbance are the frequency response functions (FRFs) $H_{11}$, $H_{21}$, and $H_{31}$. Through a similar procedure, $H_{kl}$ ($k=1,2,3$; $l=2,3$) can also be calculated by separately giving an impulse in the pitch and roll directions. As a result, all elements of the FRFs matrix $[H]_{3x3}$ of the system are obtained.

From Eq.(5), relationships between the FRFs and the modal parameters can be found as [5]

$$\left[\overline{H}\right]_{3\times 3} = \sum_{j=1}^{3}\left[\frac{\{\varphi\}_j\{\varphi\}_j^T}{\mathrm{i}(\mathrm{i}\omega - s_j)} - \frac{\{\varphi^*\}_j\{\varphi^*\}_j^T}{\mathrm{i}(\mathrm{i}\omega - s_j^*)}\right] \tag{8}$$

where

$$s_j = -2\pi\xi_j f_j + \mathrm{i}2\pi\sqrt{1-\xi_j^2}\, f_j \tag{9}$$

in which $\xi_j$, $f_j$ and $\{\varphi\}_j$ are the modal damping ratio, frequency and shape of mode $j$. The multiple input/multiple output(MIMO) orthogonal rational fractional polynomial method, briefly described as follows, is adopted to estimate the modal parameters $\xi_j$, $f_j$ and $\{\varphi\}_j$. First, we can write $\left[\overline{H}\right]_{3\times3}$ as

$$\left[\overline{H}\right]_{3\times3} = \frac{[N(s)]_{3\times3}}{[D(s)]_{3\times3}} \tag{10}$$

where $D(s)$ and $N(s)$ are orthogonal polynomials of order $2$ and $1+n_a$ respectively, and where $n_a$ is an additional order to compensate for noise effects ($n_a \geq 0$). An error function can be constructed as

$$[\varepsilon(s)] = [H][D(s)] - [N(s)] \tag{11}$$

Let $s=\mathrm{i}2\pi f$, then by use of the least square method, the norm of the errors in a specified frequency band, from frequency $f_L$ to $f_U$, is minimized. The coefficient matrices of the polynomials can be estimated. The six roots (poles) $s_j$ ($j=1,2,\ldots6$) can be found from $|[D(s)]|=0$. The corresponding residue matrix $\{\varphi\}_j\{\varphi\}_j^T$ can be calculated by the equation

$$\{\varphi\}_j\{\varphi\}_j^T = \mathrm{i}\left.\frac{[N(s)]}{\mathrm{d}[D(s)]/\mathrm{d}s}\right|_{s=s_j}, \; j=1,2,3. \tag{12}$$

Three estimations of each $\{\varphi_j\}$ can be directly obtained from Eq.(12), and the averaged results are then used as the final estimation of the mode shape $\{\varphi_j\}$.

### 2.3 Estimation of the physical matrices

The estimated modal parameters should satisfy the following orthogonality properties

$$[\Psi]^T[A][\Psi] = \mathrm{i}\begin{bmatrix}[I] & 0\\ 0 & -[I]\end{bmatrix} \tag{13}$$

$$[\Psi]^T[B][\Psi] = \begin{bmatrix}-\mathrm{i}[\Lambda] & 0\\ 0 & \mathrm{i}[\Lambda]^*\end{bmatrix} \tag{14}$$

where

$$[A] = \begin{bmatrix}C & M\\ M & 0\end{bmatrix}_{6\times6}, \quad [B] = \begin{bmatrix}K & 0\\ 0 & -M\end{bmatrix}_{6\times6} \tag{15}$$

$$[\Psi]=\begin{bmatrix}[\phi] & [\phi]^* \\ [\phi][\Lambda] & [\phi]^*[\Lambda]^*\end{bmatrix},\ [\phi]=[\{\varphi\}_1,\{\varphi\}_2,\{\varphi\}_3],\ [\Lambda]=\begin{bmatrix}s_1 & & \\ & s_2 & \\ & & s_3\end{bmatrix},\ [I]=\begin{bmatrix}1 & & \\ & 1 & \\ & & 1\end{bmatrix} \quad (16)$$

Using Eqs.(13) and (14), we can express the physical (mass, stiffness and damping) matrices in combinations as

$$\begin{bmatrix}C & M\\ M & 0\end{bmatrix}=\mathrm{i}[\Psi]^{-T}\begin{bmatrix}[I] & \\ & -[I]\end{bmatrix}[\Psi]^{-1} \quad (17)$$

$$\begin{bmatrix}K & 0\\ 0 & -M\end{bmatrix}=[\Psi]^{-T}\begin{bmatrix}-\mathrm{i}[\Lambda] & 0\\ 0 & \mathrm{i}[\Lambda]^*\end{bmatrix}[\Psi]^{-1} \quad (18)$$

For the suspension-slider-air bearing system, the estimated [*M*], [*K*] and [*C*] are effective mass, stiffness and damping matrices of the system. If we ignore the effect of the suspension on the mass matrix, the differences between the estimated *[M]* and the mass matrix *[Mc]* calculated from slider's dimensions and density will indicate the errors in the estimated mode shapes. If there are errors in the modal shapes (even very small errors, that are unavoidable), the estimated matrices will be inaccurate. The following procedure is proposed to improve the accuracy of the matrices.

1) Based on the differences between *[M]* and *[Mc]*, a correction matrix *[U]* can be found from equation

$$[Mc]=[U]^T[M][U] \quad (19)$$

2) The matrices *[K]* and *[C]* are then updated by *[U]* as

$$[K_U]=[U]^T[K][U] \quad (20)$$

$$[C_U]=[U]^T[C][U] \quad (21)$$

3) Using the matrices *[Mc]*, $[K_U]$ and $[C_U]$, updated modal parameters $f_{Uj}$, $\xi_{Uj}$, and $\varphi_{Uj}$ ($j=1,2,3$) can be calculated. Then an error parameter $\sigma$ is defined as

$$\sigma=\sum_{j=1}^{3}\left[(\xi_{Uj}-\xi_j)/\xi_j\right]^2 \quad (22)$$

4) If $\sigma$ is larger than a specified value, such as $1\times10^{-5}$, then $\varphi_j$ is replaced by $\varphi_{Uj}$ ($j=1,2,3$), and the physical matrices are calculated again by Eqs.(17) and (18). The resulting matrices are used as the new updated matrices, and we go back step 3).

5) When $\sigma$ is less than the specified value, the iteration is terminated. Simulation and calculations for dozens of cases have shown that the process converges in five or ten iterations.

## 3. Dynamic Characteristics of Five Typical ABS Designs

The dynamic characteristics of the taper-flat (TF) slider, as the simplest ABS design, was first investigated. Then, four more complicated designs were calculated. These are the H-shape negative pressure slider (TFN), the transverse pressure contour slider (TFS), the shaped rail slider(TFB), and the authors' proposed transverse grooved slider (TFT). In order to properly compare their dynamics characteristics, all sliders were designed as: 50% sliders (2.0×1.6×0.42 mm); with symmetry about their center line; 4 μm recess depth for all areas not covered by any of the rails; zero crown, camber and twist; 0.2 mm taper length and 10 mrad angle ; step rails as vertical wall profiles. The ambient pressure and viscosity are 1.014e5 pa and 1.806e-5 nsm$^{-2}$, respectively. The mass matrices of all sliders with respect to their center are

$$[Mc]=\begin{bmatrix} 5.952\times10^{-6} & 0 & 0 \\ 0 & 2.176\times10^{-12} & 0 \\ 0 & 0 & 1.361\times10^{-12} \end{bmatrix} \text{ (kg, m)} \qquad (23)$$

The slider speed relative to the disk is first chosen as 14.14 m/s (5400 RPM, at the radial position of 25 mm) and with zero skew angle. The normal load is 3.5 gram. The ABS's of all sliders were modified to achieve steady flying heights of about 48 nm at the center of the trailing edge. To focus the research on the slider-air bearings, we ignored the effects of the suspensions (by specifying the suspensions to have very small stiffness and damping coefficients). After the systems were identified and in order to investigate the separate effects of the relative speed and skew angle on the dynamics properties, we compared the

modal parameters at 10.47 m/s with zero skew angle (4000 RPM, 25 mm), 17.80 m/s with zero skew angle (6800 RPM, 25 mm), $-10^o$ skew angle (5400 RPM, 25 mm), and $10^o$ skew angle (5400 RPM, 25 mm). The defined direction of the skew angle is different from the definition in the IDEMA standards manual. Here, the skew angle decrease from the ID to the OD. The figures show the results for the five sliders with the same format and scale to make the comparisons easy.

Because the stiffness and damping of the system are described as the 3x3 matrices, it is inconvenient to compare the stiffness and damping for the different designs by the metrics. Since the systems have a same mass matrix shown in Eq.(23), the modal frequencies and damping ratios of the systems will directly indicate the differences in the stiffness and damping of the systems, Therefore, we compared the frequencies and damping rations instead of the matrices.

### 3.1 The taper-flat slider

We found that the time step used in the calculation of the dynamic responses has significant effects on the results, especially on the modal damping ratios. The calculated damping ratios of the taper-flat slider using several different time steps are shown in Figure 2. The figure shows that the time step as small as 0.1 μsecond is required to give the converged values. The 0.1 μsecond time step will be used in all of the following calculations. For the stiffer bearings, such as in the 30% sliders, a even smaller step may be needed. In a previous report [5], the time step was 1.0 μsecond, thus the damping ratios are over estimated.

The ABS of the taper flat slider (TF), and the steady flying state pressure profiles are shown in Figure 3 a) and b). The width of each rail is .154 mm. The estimated modal parameters and the physical matrices are shown in Figure 3c). The smallest damping ratio is 1.94%. The estimated mass matrix is very close to *[Mc]*, given in Eq. 23. That indicates

the estimated modal shapes have very good accuracy. Figure 3d) shows the nodal lines of the three mode shapes. We can see that the slider has a pure roll mode, and no pure vertical and pitch modes. The first two modes are coupled modes between the vertical motion and the pitch motion. The slider has the some mode shapes at the three different speeds, but it has very different shapes for modes 2 and 3 for the different skew angles, as shown in Figure 3 e) and f).

Figure 4 shows the effects of speed and skew angle on the FH, modal frequencies and damping ratios of the system. The solid lines in the figures represent the effects of the speed at the fixed skew angle of zero degree. We can see that the changes of the FH, the frequencies and the ratios are almost linearly related to the speed in the range from 10.47m/s to 17.8m/s. As the speed is increased, the FH is increased, the frequencies are decreased, and the damping ratios are increased. The dotted lines represent the effects of the skew angle at the fixed speed of 14.14 m/s. The skew angle significantly affects the FH, the frequencies and the damping ratios. The effects of speed and skew angle show that flying at a higher FH will be accompanied by a softer air-bearing with larger damping.

### 3.2 The H-shape negative pressure slider (TFN)

The first conventional negative pressure (sub-ambient) slider, which was proposed by Garnier et al. [6], is the H-shape slider. Many researchers, as reported in [7, 8, 11, 16], investigated its properties. Sliders with negative pressure are widely used in current drives, because they have many advantages, such as faster take-off, less speed sensitivity, better altitude insensitivity, smaller normal load (lower friction during start-up and landing), and lower FH sensitivity to tolerances. The main disadvantage is a higher potential for contamination.

The ABS of the H-shape slider studied here, and the steady flying state pressure profile are shown in Figure 5 a) and b). The width of each long rail is .25 mm, and the cross rail starts

at 0.4 mm from the leading edge and is 0.2 mm wide. All of the results are shown in Figures 5 and 6. Comparing the TFN slider with the TF slider, we find that the TFN slider has the following properties: ❶ Much higher modal frequencies, which means that the slider has a much stiffer air bearing. ❷ Very small damping ratios, the smallest ratio is only 0.76%. Figure 7 shows the dynamic responses under impulse excitations in the vertical and roll directions (the impulse velocities are .002 m/s and 2 rad/s, respectively). As seen, the responses take a relatively long time to be damped out. If the suspension can not provide sufficient damping, the slider could be dynamically unstable, or have large fluctuations. ❸ The frequencies of modes 2 and 3 are too close to each other and generate a beating phenomenon (shown in Figure 7) increasing the time for damping out the disturbance. ❹ Low sensitivity of the FH, frequencies and damping ratios to the speed. ❺ Very high sensitivity of the FH and the frequencies to the skew angle. Low sensitivity to speed and high sensitivity to skew angle results in a large change of the FH from the ID to the OD in the drive.

**3.3 The transverse pressure contour slider (TFS)**

The transverse pressure contour slider, which was first proposed by White [9] and named TPC, has a stepped rail geometry. The slider is known for having constant FH from the ID to the OD. The ABS of the slider used here is shown in Figure 8 a). The total width of each rail is 0.3 mm and they have 0.5 μm recess, the narrower rail starts at 0.045 mm from the outer edge and is 0.148 mm wide. All of the results are shown in Figures 8 and 9. Comparing the TFS slider with the TF slider, we see that the TFS slider has the following properties: ❶ Similar modal frequencies and modal shapes except the frequency of the roll mode is smaller than that of the TF slider, which means the TFS slider has lower stiffness in the roll direction. ❷ Higher damping ratios, the smallest ratio is about 2.5%, and the largest one is 7%, which means the TFS slider has good dynamic stability. ❸ High sensitivity of the FH, frequencies and damping ratios to speed and skew angle. The damping ratio of the roll mode rapidly increases with increase in speed . ❹ Constant FH

from the ID to the OD is achievable because the effects of the speed and the angle can just compensate each other if the initial skew angle is properly designed.

### 3.4 The shaped rail slider(TFB)

The shaped rail slider is also widely used in current drives. The shaped rail improves the performance giving constant FH from the ID to the OD and at different altitudes. The Bow Tie slider [11], as a typical sample of the shaped rail sliders, was calculated here for comparison of its dynamic properties with the TF slider. The ABS of the slider, and the steady flying state pressure profiles are shown in Figure 10 a) and b). The two rails have 0.275 mm width at the leading and trailing edges and 0.075 mm width at the center. Comparing the TFB slider with the TF slider, we find that the TFB slider has the following properties, as shown in Figures 10 and 11: ❶ Similar modal frequencies and damping ratios. ❷ The modal frequencies of mode 2 and mode 3 are too close to each other and generate a beating phenomenon, increasing the time for damping out disturbances. ❸ No pure roll mode was found, which may be a natural property of the slider, or it may indicate a larger calculation error for the frequencies of modes 2 and 3, which are very close to each other. ❹ Much lower sensitivity of the FH, frequencies and damping ratios to skew angle. A better FH profile than that of the TF slider is expected.

### 3.5 The transverse grooved slider (TFT)

Large damping is always important for dynamic stability and faster slider settling. Therefore, high damping becomes a design objective of sliders. Comparing the pressure profiles of the previous four sliders, we can see that the sliders with the smoother pressure profiles have smaller damping ratios, and the rougher profiles have larger damping. That means the damping of the slider-air bearings is directly related to the gradient of the pressure. Indeed, it is the transverse viscous shear in the bearings of the TFS slider that dissipates vibration energy [9,13]. The vibratory motion of the slider causes a pressure driven viscous transverse flow back and forth across the stepped rails, and dampens the

motion. If the rails are grooved in the transverse direction, the viscous shear will be more significant. Moreover, the pressure gradient will be greatly increased if the rails are grooved in the transverse direction. Based on these considerations, we designed a transverse grooved slider (TFT). The ABS of this slider is shown in Figure 12 a). The width of each rail is 0.166 mm. There are three small rectangular recesses of 0.5 μm depth on each rail. The recesses are 0.15 mm long and start at 0.85, 1.30 and 1.75 mm, respectively, from the leading edge of the slider. The steady FH is 47.53 nm at 14.14 m/s speed and zero skew angle. The pressure profile is shown in Figure 12 b). We can see that there is the larger pressure gradient in the bearing, and therefore larger damping is to be expected.

Figure 12 c)-f) and Figure 13 show all of the simulation results for the TFT slider. Comparing the TFT slider with the TF slider, we see that the TFT slider has the following properties: ❶ Similar modal frequencies and modal shapes. ❷ Much higher damping ratios, especially the damping ratio of mode 2 is changed from 1.94% to 4.48%, an increase of about 130%. ❸ Higher sensitivity of the FH, frequencies and damping ratios to the speed, and lower sensitivity to the skew angle. The FH varies from the ID to the OD. ❹ Comparing the TFT slider with the TFS slider, we can see that the TFS slider design mainly increases the damping ratios of the first and third modes, and the TFT slider design increases the damping ratios of all modes. In further simulations, we found that the damping ratios can be obviously increased by increasing the recess depth and adding more recesses. Moving the recesses toward the leading edge will increase the damping ratios of the first mode. This can be easily explained by the mode shapes.

## 4. Various Complicated ABS Designs and Design Guide

Each of the previous five typical ABS designs has its own advantages and disadvantages. Combinations of some of these designs is a very reasonable choice. Therefore, many complicated ABS designs have been proposed. For example, the Headway AAB slider and

NSIC "Nutcraker" slider were designed by combining the TFN design with the TFB design. The higher modal frequencies and lower damping ratios are to be expected. The TNP slider [13], combining the TFN and TFS designs, should have higher modal frequencies and damping ratios. The Seagate AAB slider [12] includes the TFN, TFS and TFB designs together. It should demonstrate various desired properties.

Considering all of the design requirements, reasonable combinations in slider designs should be as follows.

| | TFN | **and** | (TFS **and/or** TFB) and | (TFS **and/or** TFT) |
|---|---|---|---|---|
| For: | Fast take-off | | Constant FH | High damping |
| | Low normal load | | | |
| | Altitude insensitivity | | | |
| | Good tolerance | | | |
| | High stiffness | | | |

Using these combinations, designers should also be concerned with the contamination problem.

A new slider design, named the HDS slider, with a complicated ABS, which was expected to have high stiffness and damping, is shown in Figure 14. The slider combines the features of TFN, TFS, TFB and TFT. The slider has a negative pressure cavity (TFN) at the center and three step rails (TFS) on the each side. There are three rectangular recesses (TFT) at each middle step rail, and the rails are shaped. The recesses are 4 μm in the cavity and 1 μm on the lower rails. Such a complex ABS is proposed for its desired features, and its final design should be obtained by design optimization.

The steady flying attitudes at 14.14m/s and zero skew (25 mm, 5400 RPM) are 48.90 nm FH at the center of the trailing edge, 142.0 μrad pitch, and 5.94 μrad roll. The pressure profile as shown in Figure 15 has numerous high gradients. The modal parameters and the physical matrices are shown in Figure 16. For comparison, the modal frequencies and

damping ratios of the Headway AAB, "Nutcracker", TNP and HDS sliders are also shown in Table 1. The TNP slider is modified to have about 48 nm FH. Figure 17 shows the dynamic responses for the two impulse excitations (the responses to the initial velocities of .002 m/s and 2 rad/s, respectively) of the TNP and HDS sliders. We can see that the air bearing of the HDS slider has much larger damping and medium stiffness.

The FH profile of the HDS slider from the ID (23 mm, $-2^0$ skew) to the OD (47 mm, $18^0$ skew) at 5400 RPM is shown in Figure 18. The results show the HDS slider is a good initial design for high performance sliders. It is necessary to improve the FH profile through design optimization.

## 5. CONCLUSIONS

We apply the dynamic simulation and modal analysis method to analyze the dynamic properties of slider-air bearings. The multiple input /multiple output orthogonal rational fractional polynomial method was used to estimate the modal parameters of the system, and an iteration procedure was used to estimate stiffness and damping matrices.

Five typical designs, one of which is first proposed in this report, of the air bearing surfaces are briefly discussed. The dynamic characteristics of the five designs are studied, and they are compared with each other. It is found that the negative pressure slider has highest stiffness and lowest damping, the TPC and the newly proposed slider demonstrate higher damping.

The complicated ABS design problem is briefly discussed. A new slider with a complicated ABS is designed, analyzed and compared with other sliders. The designed slider is shown to have much higher damping. The results generally indicate that the proposed methods are quite powerful, and the results presented in this report are believed to be useful for high performance slider design.

## ACKNOWLEDGMENTS

This study is supported by the Computer Mechanics Laboratory at the University of California at Berkeley.

## REFERENCES

[1] Ono, K., 1975, "Dynamic Characteristics of Air-Lubricated Slider Bearing for Noncontact Magnetic Recording", J. of Lubrication Technology, pp.250-260.

[2] Smith, P. W. and Iwan, W. D., 1991, "Dynamic Figures of Merit for the Design of Gas-Lubricated Slider Bearings", ASME, Adv. in Info. Storage Syst. V.3, pp.41-53.

[3] Mitsuya, Y. and Ota, H., 1991, "Stiffness and Damping of Compressible Lubricating Films Between Computer Flying Heads and Textured Media: Perturbation Analysis Using the Finite Element Method", ASME, J. of Tribology, Vol. 113, 819-827.

[4] Hu, Y. and Bogy, D. B., 1995, "The CML Air Bearing Dynamic Simulator", Technical Report No. 95-011, Computer Mechanics Lab., Dept. of Mechanical Engineering, University of California at Berkeley.

[5] Zeng, Q.H., Chen, L.S. and Bogy, D.B., 1996, "A Modal Analysis Method for slider Air Bearings in Hard Disk Drives", CML Technical Report No. 96-021, Dept. of Mechanical Engineering, Univ. of California at Berkeley.

[6] Garnier, M. F., Tang, T. and White, J. W., 1974 "Magnetic Head Slider Assembly," U.S. Patent No. 3,855,625.

[7] Kogure K., Fukui S., Mitsuya Y. and Kaneko R., 1993, "Design of Negative Pressure Slider for Magnetic Recording Disks", Tran. of the ASME, J. of Lubrication Technology, Vol.105, pp. 496-502.

[8] White, J.W., 1983, "Flying Characteristics of the 'Zero-Load' Slider Bearing," ASME, J. of Lubrication Technology, Vol.105, pp 484-490.

[9] White, J. W., 1991, "The Transverse Pressure Contour Slider: Flying Characteristics and Comparison with Taper-Flat and Cross-Cut Type Sliders", ASME, Adv. in Info. Storage Syst., Vol. 3, pp. 1-14.

[10] Nishihira, H., Dorius, L., and Bolasna, S., 1988, "Performance Characteristics of the IBM 3380K air bearing design", Tribology and Mechanics of Magnetic Storage Systems, 5, pp. 117-123.

[11] Peck, P.R., Wang, B. S., Park, K.O. and Jhon, M. S., 1995, "Scaling Criteria for Slider Miniaturization Including Shape Effects," Proc. Sixth Intl. Symp. Adv. Infr. Storage Proc. system, ISPS-Vol. 1, pp1-6.

[12] Hardie, C, Menon, A., Crane, P. and Egbert, D., 1994, "Analysis and Performance Characteristics of the Seagate Advanced Air Bearing Slider", IEEE Tran. Vol.30, pp424-432.

[13] White, J. W., 1996, "Flying Characteristics of the Transverse and Negative Pressure Contour ('TNP") Slider Air Bearing", ASME, 96-Trib-8.

[14] Hu, Y. and Bogy, D. B., 1996, "Dynamics Stability and Spacing Modulation of Sub-25 nm Fly Height Sliders", ASME, 96-Trib-56.

[15] Suzuki, S., and Nishihira, H., 1995, "Study of Slider Dynamics over Very Smooth Magnetic Disks", J. of Tribology (95-Trib-38)).

[16] Kang, S. C., Peck, P. R., Jhon, M. S., and Kim, I. E., 1995, "Transient Behavior of Negative Pressure Sliders over Rough Surfaces Including Comparisons with Positive Pressure Sliders", Proc. Sixth Intl. Symp. Adv. Infr. Storage Proc. system, ISPS-Vol. 1, pp 7-12.

| Sliders | FH (nm) | Mode 1 | | Mode 2 (Roll) | | Mode 3 | |
|---|---|---|---|---|---|---|---|
| | | Freq. (kHz) | Damp (%) | Freq. (kHz) | Damp (%) | Freq. (kHz) | Damp (%) |
| HDS | 48.9 | 56.22 | 5.23 | 82.27 | 5.19 | 91.72 | 3.86 |
| TNP | 48.47 | 58.16 | 4.46 | 93.12 | 2.03 | 99.92 | 1.54 |
| "Nutcracker" | 34.23 | 55.04 | 3.11 | 84.42 | 1.69 | 125.1 | 1.17 |
| Headway AAB | 40.71 | 49.11 | 3.05 | 102.2 | 0.94 | 105.9 | 1.11 |

Table 1 Modal frequencies and damping ratios of the sliders at 14.14 m/s and zeor skew

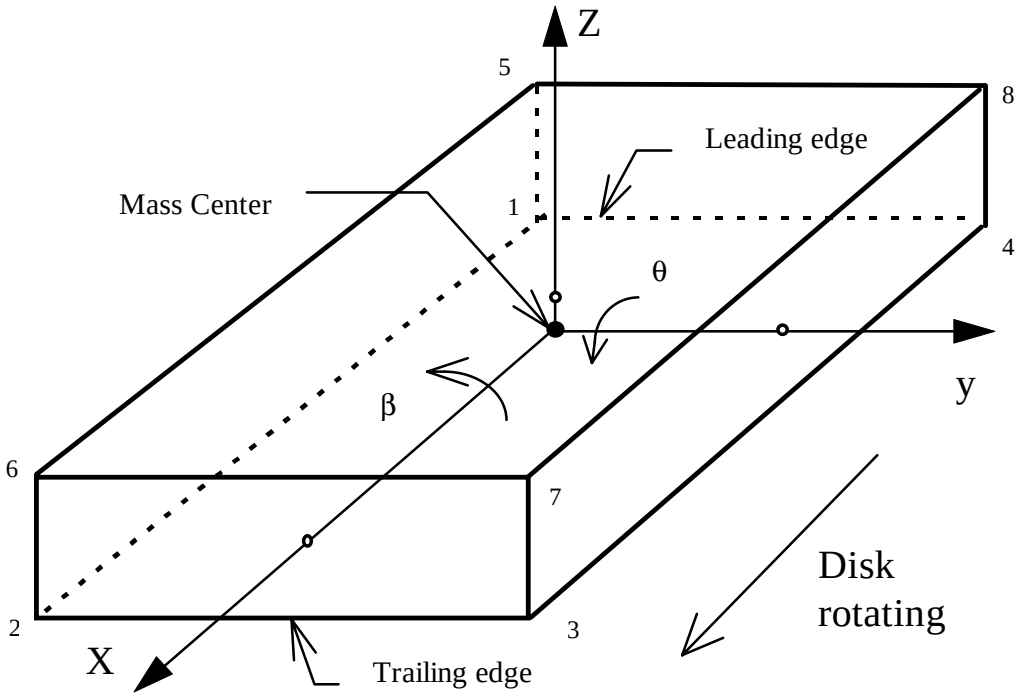


Figure 1 Schematic diagram of the slider geometry and coordinate system

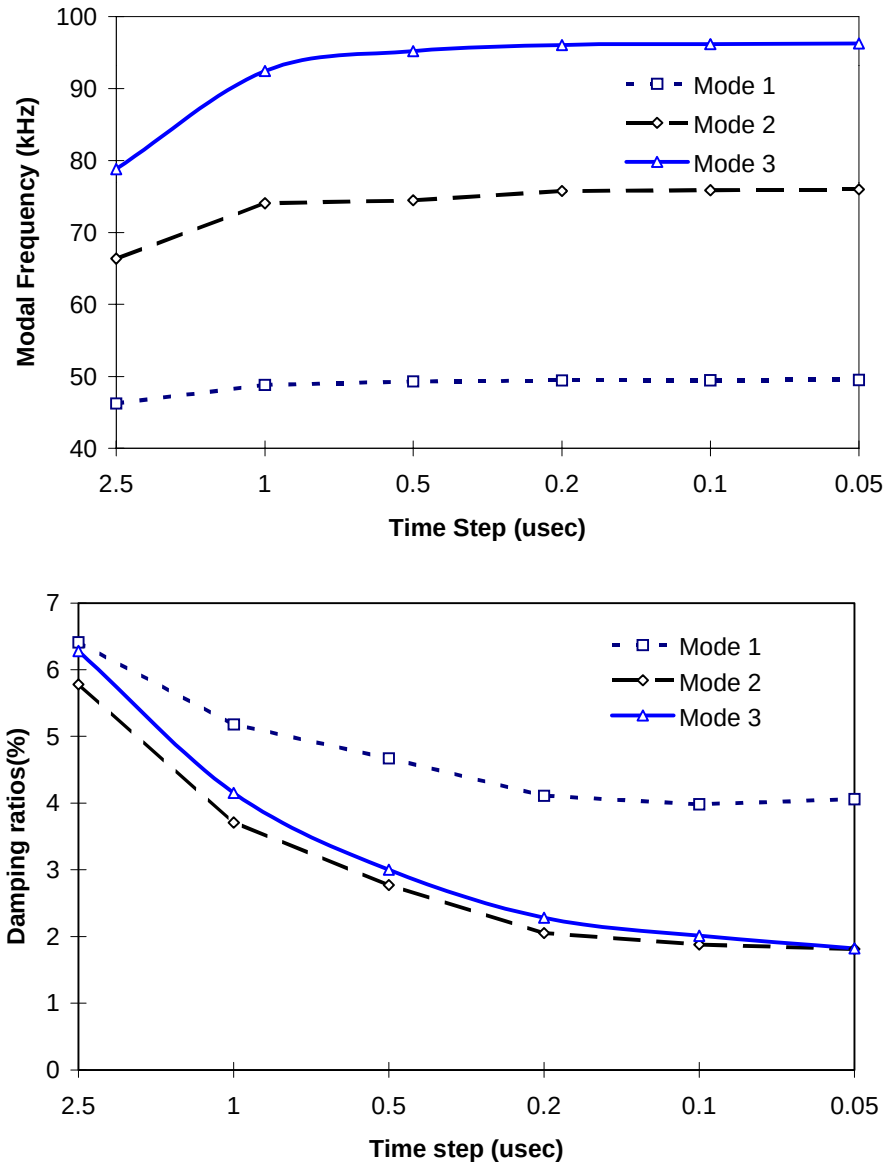


Figure 2 Modal frequencies and damping ratios vs the time step used in the calculations

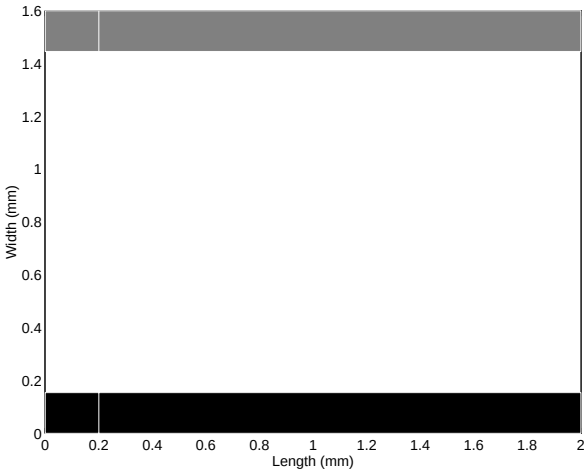


a) Rails

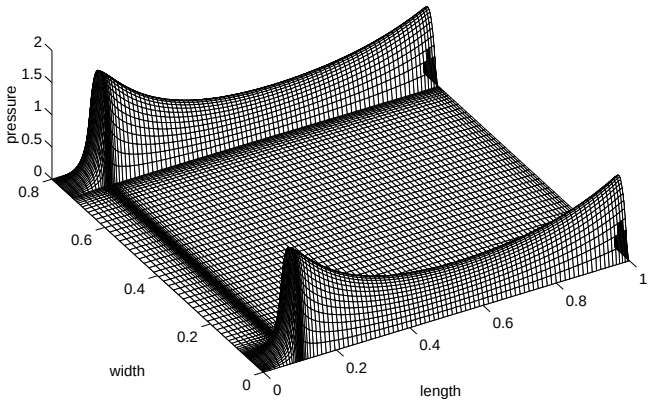


b) Pressure profile

Results Table

Name: tf540 Flying height=47.81 nm

| Mode | 1 | | 2 | | 3 | |
|---|---|---|---|---|---|---|
| Freq.(Hz) | 49.51 | | 75.98 | | 96.2 | |
| Damp(%) | 3.97 | | 1.94 | | 2.004 | |
| | Amp. | Phase | Amp. | Phase | Amp. | Phase |
| | 3.616e−01 | −0.07 | 3.061e−01 | −179.89 | 2.043e−02 | 177.38 |
| | 6.230e+02 | 0.00 | 4.855e+02 | −0.00 | 3.209e+01 | −2.82 |
| | 1.399e+00 | 55.20 | 6.494e+01 | 177.52 | 7.798e+02 | 0.00 |

| | Physical Matrices | | | Updated Matrices | | |
|---|---|---|---|---|---|---|
| | 5.84e−06 | 3.23e−11 | 8.78e−13 | 5.952e−06 | −1.361e−26 | 0.000e+00 |
| Mass | 3.23e−11 | 2.14e−12 | −1.25e−15 | −2.878e−25 | 2.176e−12 | 3.631e−29 |
| | 8.78e−13 | −1.25e−15 | 1.35e−12 | 7.279e−27 | 3.951e−29 | 1.361e−12 |
| | 9.63e+05 | −2.28e+02 | −2.05e+01 | 9.811e+05 | −2.371e+02 | −2.133e+01 |
| Stiff. | −2.28e+02 | 3.41e−01 | 1.13e−02 | −2.371e+02 | 3.494e−01 | 1.139e−02 |
| | −2.05e+01 | 1.13e−02 | 4.93e−01 | −2.133e+01 | 1.139e−02 | 4.964e−01 |
| | 1.282e−01 | 9.879e−06 | 1.028e−06 | 1.295e−01 | 1.124e−05 | 8.844e−07 |
| Damp. | 9.879e−06 | 4.623e−08 | 7.582e−11 | 1.124e−05 | 4.659e−08 | 1.807e−10 |
| | 1.028e−06 | 7.582e−11 | 3.245e−08 | 8.844e−07 | 1.807e−10 | 3.306e−08 |

c) Result table

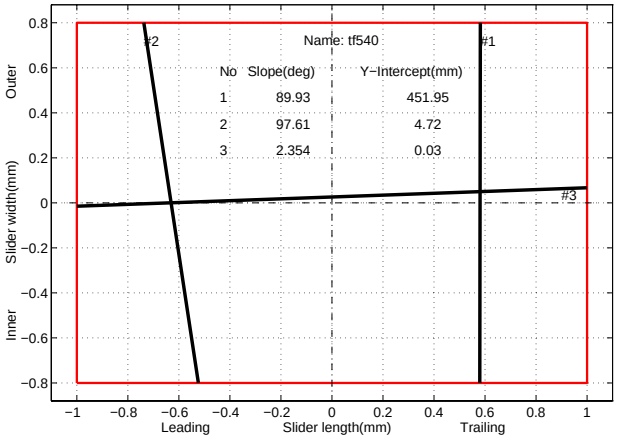


d) Nodal lines (14.14 m/s, 0 skew angle)

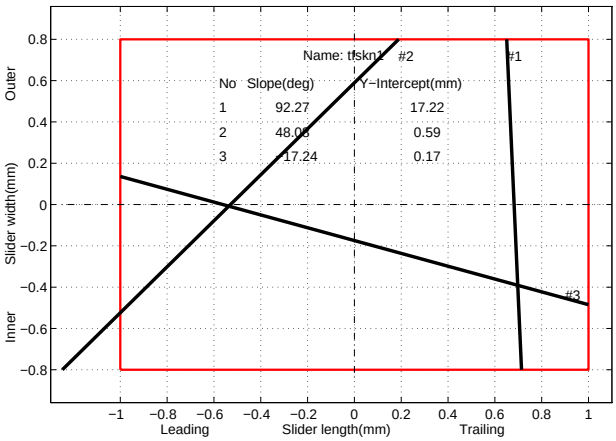


e) Nodal lines (14.14m/s, -10 skew angle)

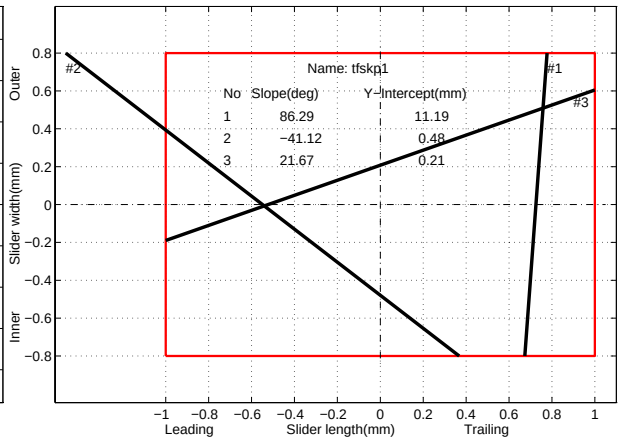


f) Nodal lines (14.14 m/s, 10 skew angle)

Figure 3 The taper-flat slider (TF) and its results

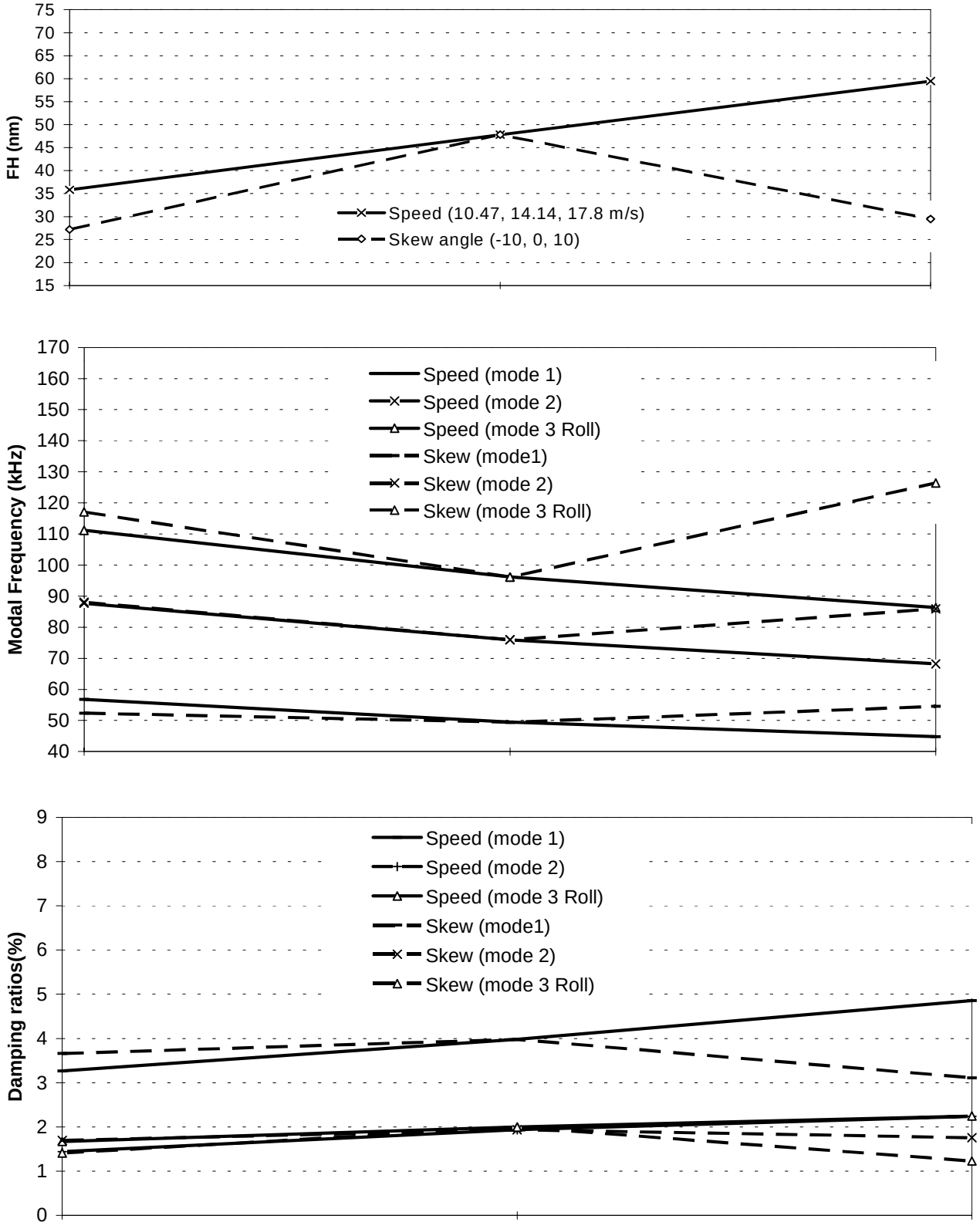


Figure 4 FH, Frequency and damping ratio vs the speed and skew angle of slider TF

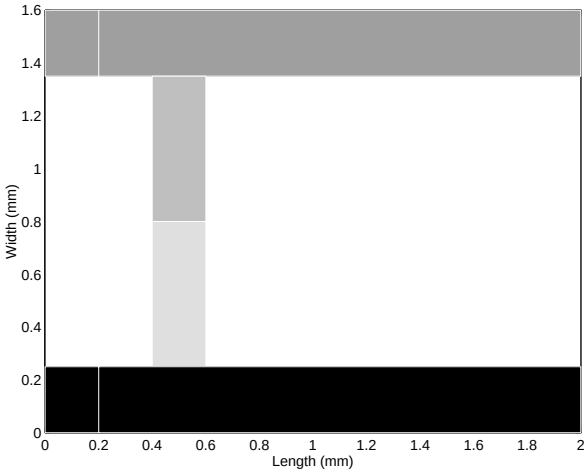


a) Rails

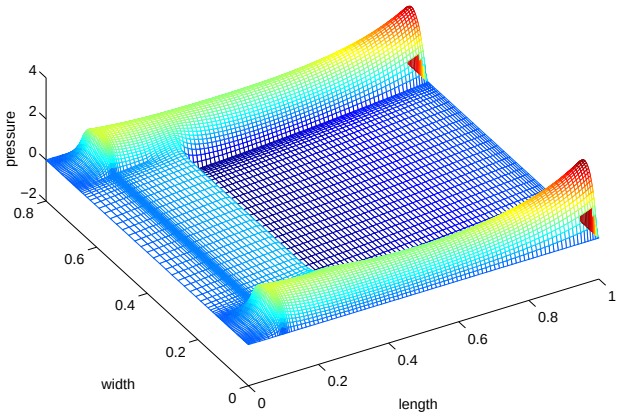


b) Pressure profile

Results Table

Name: tfn540 Flying height=47.02 nm

| Mode | 1 | | 2 | | 3 | |
|---|---|---|---|---|---|---|
| Freq.(Hz) | 68.45 | | 113.2 | | 126.3 | |
| Damp(%) | 2.564 | | 0.7621 | | 0.9352 | |
| | Amp. | Phase | Amp. | Phase | Amp. | Phase |
| | 3.258e−01 | −0.00 | 2.279e−01 | 178.92 | 3.807e−02 | 178.73 |
| | 4.908e+02 | 0.00 | 4.137e+02 | 0.00 | 6.961e+01 | −1.78 |
| | 9.162e−01 | 130.74 | 1.247e+02 | 178.20 | 6.679e+02 | −0.00 |

| | Physical Matrices | | | Updated Matrices | | |
|---|---|---|---|---|---|---|
| | 5.97e−06 | 1.13e−11 | 9.62e−13 | 5.952e−06 | 7.237e−27 | 6.032e−28 |
| Mass | 1.13e−11 | 2.18e−12 | −4.10e−16 | 1.527e−25 | 2.176e−12 | 8.385e−29 |
| | 9.62e−13 | −4.10e−16 | 1.37e−12 | −2.028e−26 | 1.218e−28 | 1.361e−12 |
| | 1.98e+06 | −5.80e+02 | −3.97e+01 | 1.975e+06 | −5.819e+02 | −4.012e+01 |
| Stiff. | −5.80e+02 | 7.90e−01 | 2.71e−02 | −5.819e+02 | 7.899e−01 | 2.714e−02 |
| | −3.97e+01 | 2.71e−02 | 8.58e−01 | −4.012e+01 | 2.714e−02 | 8.525e−01 |
| | 2.799e−02 | 4.576e−05 | −6.668e−06 | 6.262e−02 | 2.261e−05 | −2.730e−06 |
| Damp. | 4.576e−05 | 3.321e−08 | 6.899e−10 | 2.261e−05 | 4.830e−08 | −1.888e−09 |
| | −6.668e−06 | 6.899e−10 | 1.831e−08 | −2.730e−06 | −1.888e−09 | 2.047e−08 |

c) Result table

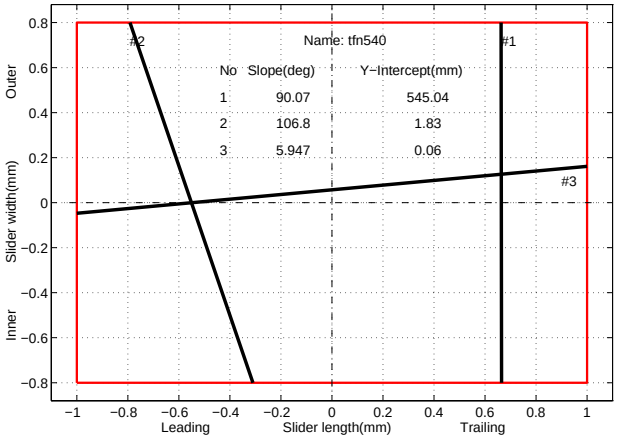


d) Nodal lines (14.14 m/s, 0 skew angle)

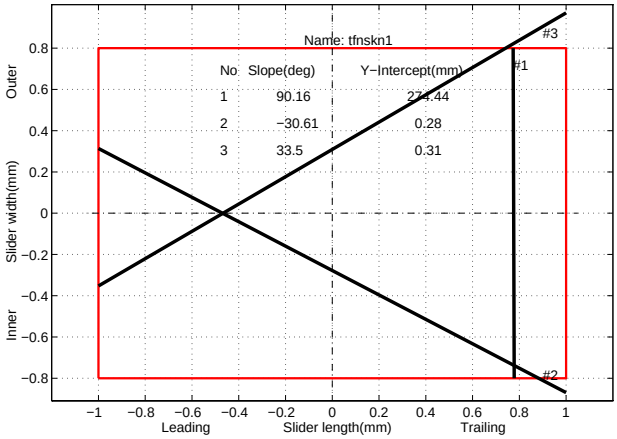


e) Nodal lines (14.14m/s, -10 skew angle)

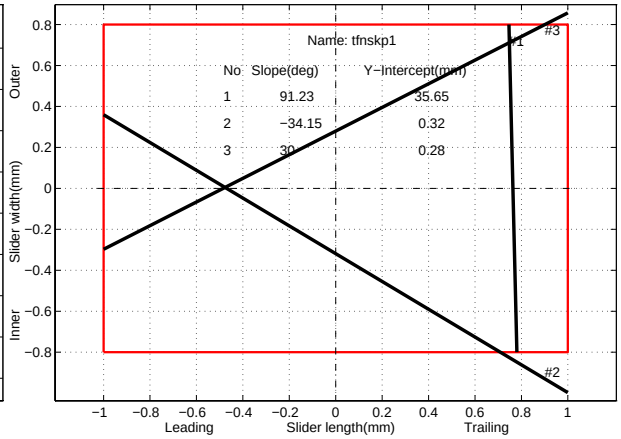


f) Nodal lines (14.14 m/s, 10 skew angle)

Figure 5 The H-shape negtive pressure slider (TFN) and its results

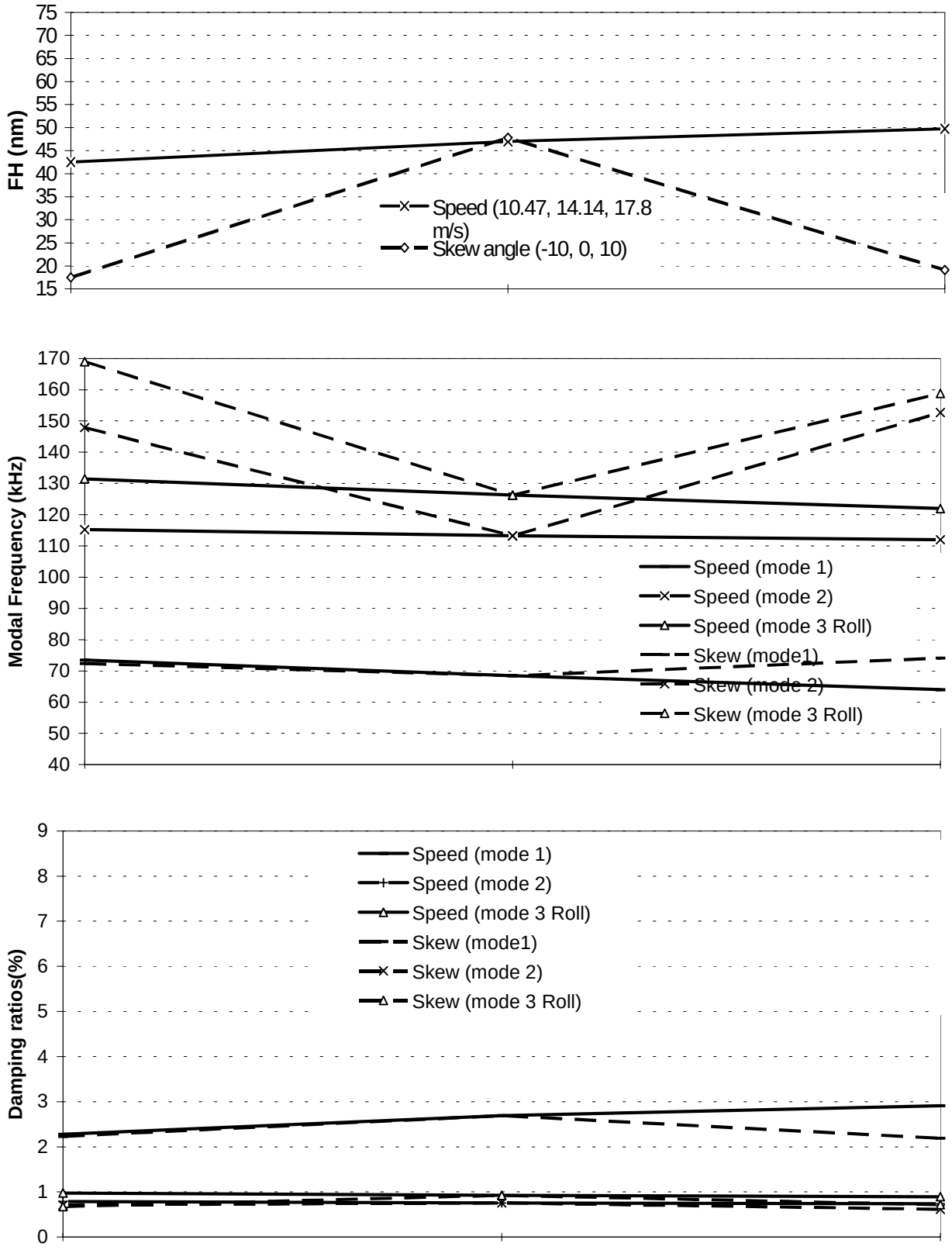


Figure 6 FH, Frequency and damping ratio vs the speed and skew angle of slider TFN

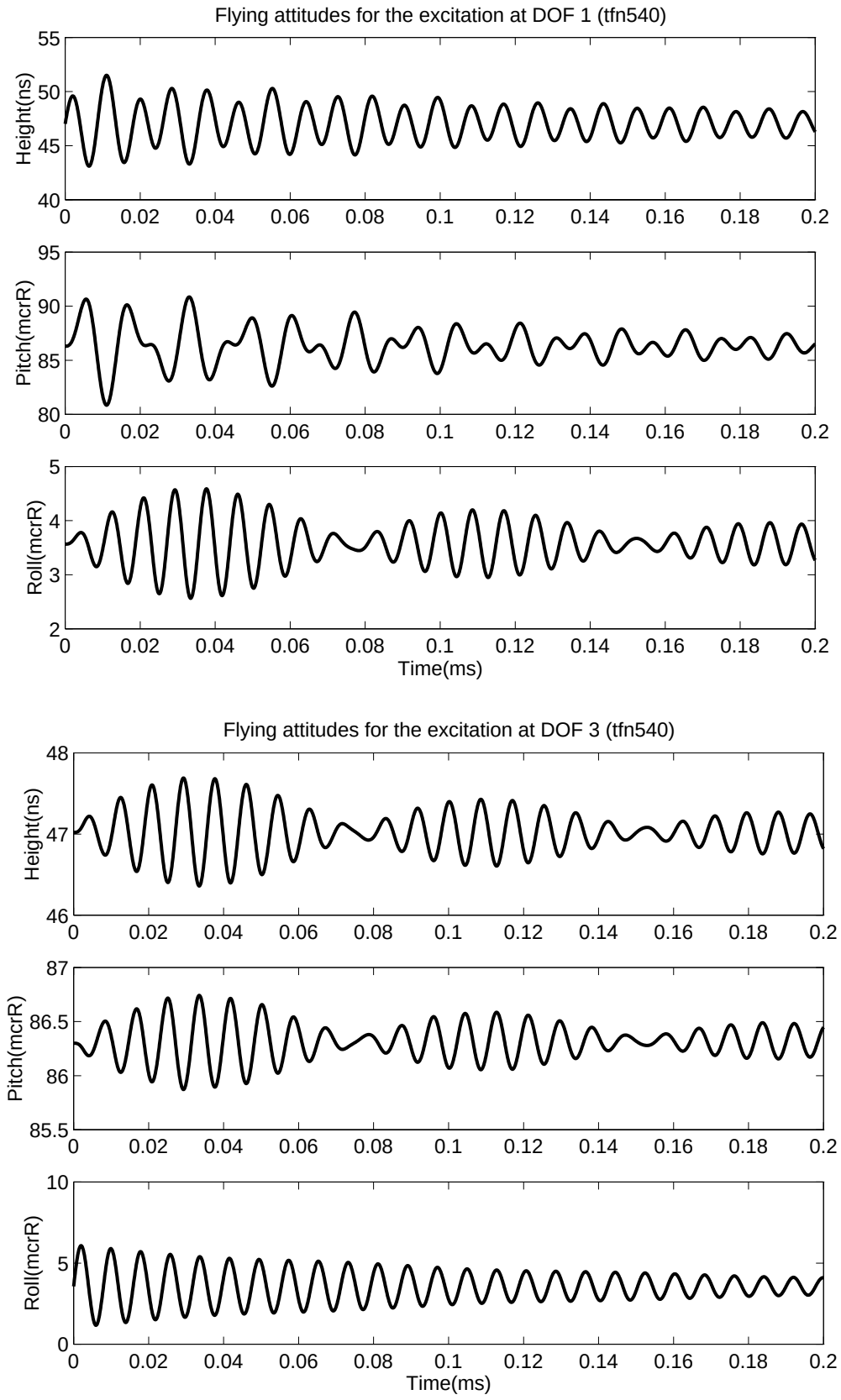


Figure 7 The dynamic responses of the TFN slider for the vertical and pitch exctitaions

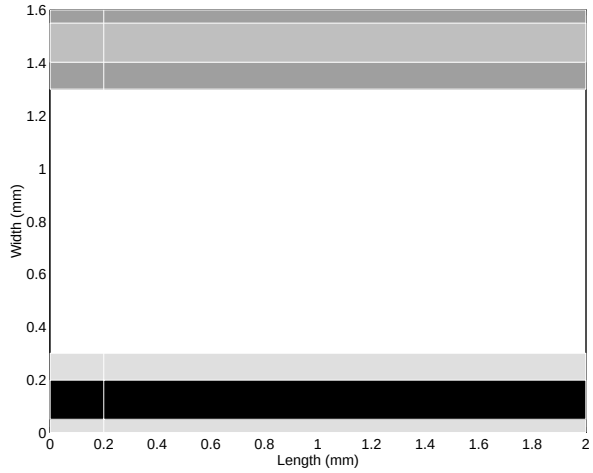


a) Rails

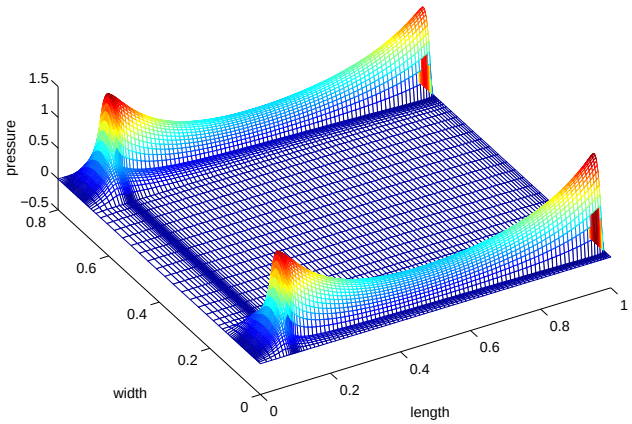


b) Pressure profile

Results Table

Name: tfs540 Flying height=131.1 nm

| Mode | 1 | | 2 | | 3 | |
|---|---|---|---|---|---|---|
| Freq.(Hz) | 45.76 | | 74.69 | | 85.21 | |
| Damp(%) | 6.965 | | 2.487 | | 3.001 | |
| | Amp. | Phase | Amp. | Phase | Amp. | Phase |
| | 3.919e−01 | −0.62 | 2.894e−01 | 179.88 | 4.327e−02 | −167.18 |
| | 6.270e+02 | −0.01 | 4.949e+02 | 0.00 | 8.760e+01 | 30.64 |
| | 4.288e+00 | −63.94 | 1.312e+02 | 173.84 | 8.196e+02 | 0.00 |

| | Physical Matrices | | | Updated Matrices | | |
|---|---|---|---|---|---|---|
| | 5.92e−06 | −3.79e−11 | 6.74e−12 | 5.952e−06 | 7.358e−28 | −1.625e−27 |
| Mass | −3.79e−11 | 2.17e−12 | −1.68e−14 | 6.308e−26 | 2.176e−12 | 1.460e−28 |
| | 6.74e−12 | −1.68e−14 | 1.35e−12 | −3.516e−26 | 1.269e−28 | 1.361e−12 |
| | 8.92e+05 | −2.54e+02 | −1.46e+01 | 8.971e+05 | −2.492e+02 | −2.085e+01 |
| Stiff. | −2.54e+02 | 3.36e−01 | 7.15e−03 | −2.492e+02 | 3.340e−01 | 6.284e−03 |
| | −1.46e+01 | 7.15e−03 | 3.85e−01 | −2.085e+01 | 6.284e−03 | 3.878e−01 |
| | 1.814e−01 | 6.172e−06 | −5.655e−05 | 1.823e−01 | 8.546e−06 | −5.692e−05 |
| Damp. | 6.172e−06 | 8.441e−08 | 7.075e−08 | 8.546e−06 | 8.198e−08 | 7.166e−08 |
| | −5.655e−05 | 7.075e−08 | 3.869e−08 | −5.692e−05 | 7.166e−08 | 4.200e−08 |

c) Result table

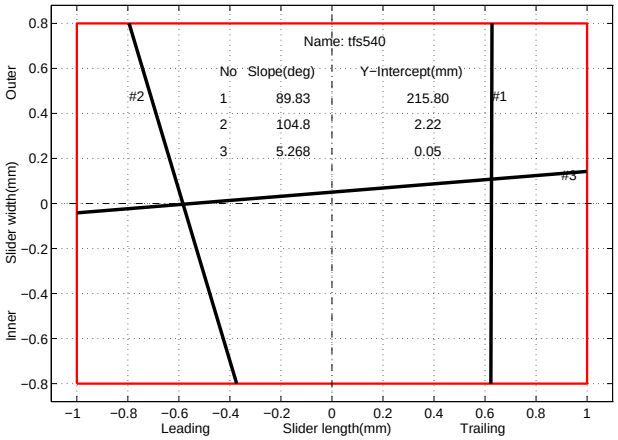


d) Nodal lines (14.14 m/s, 0 skew angle)

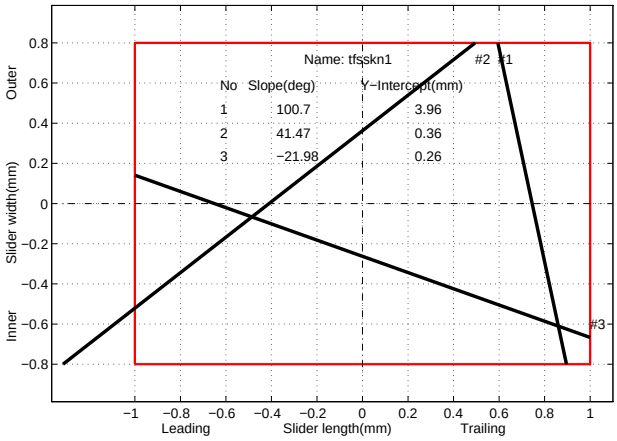


e) Nodal lines (14.14m/s, -10 skew angle)

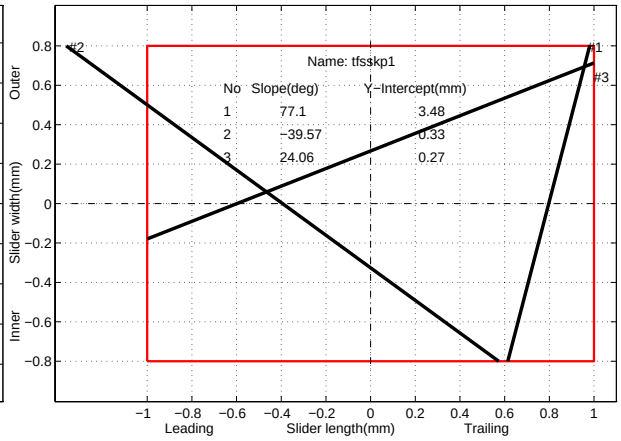


f) Nodal lines (14.14 m/s, 10 skew angle)

Figure 8 The transverse pressure slider (TFS) and its results

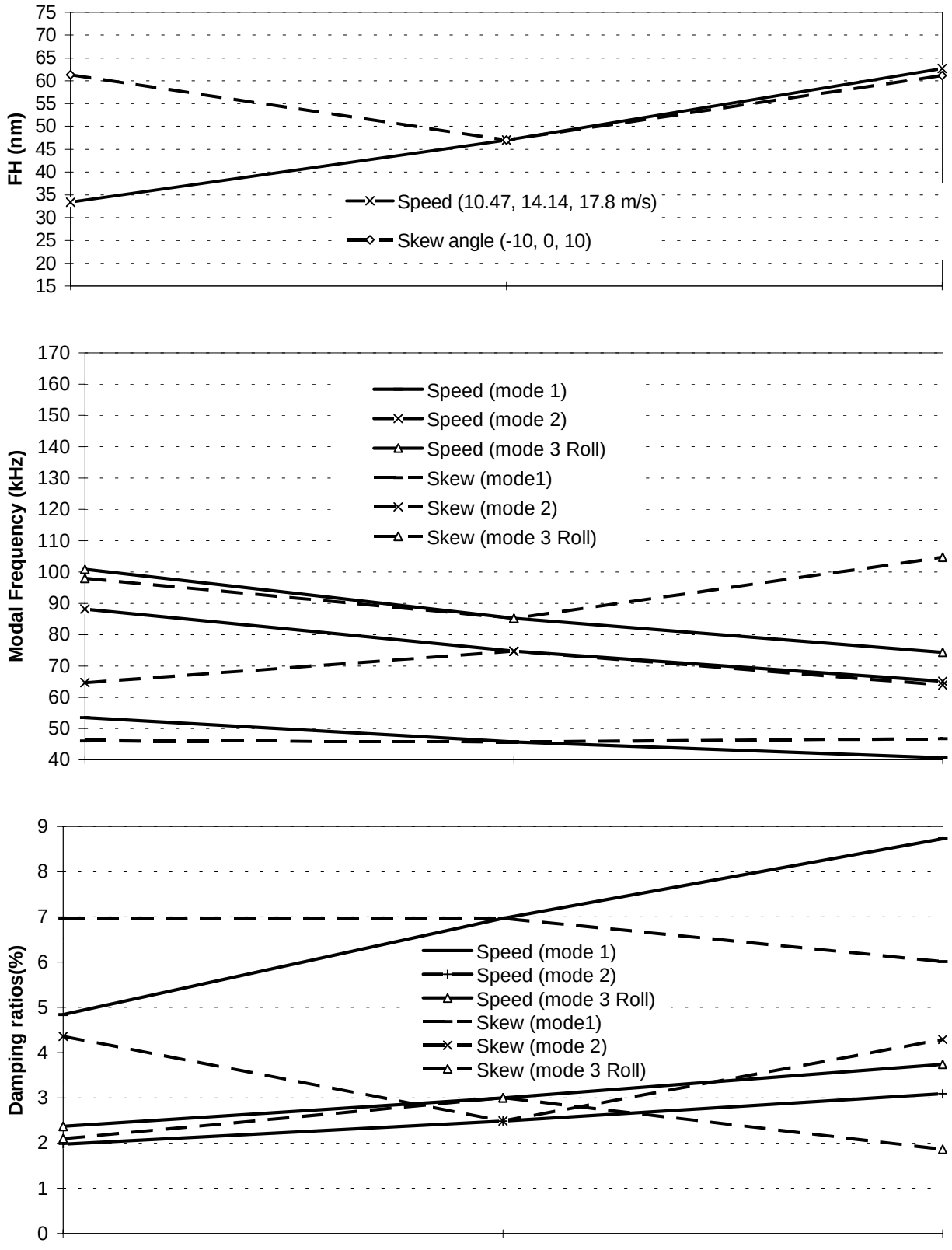


Figure 9 FH, Frequency and damping ratio vs the speed and skew angle of slider TFS

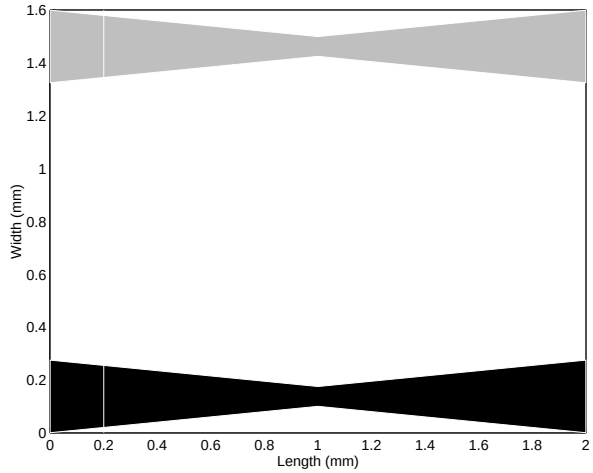


a) Rails

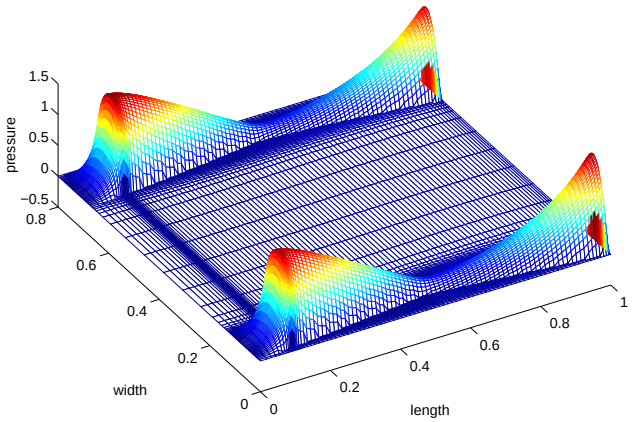


b) Pressure profile

Results Table

Name: tfb540 Flying height=47 nm

| Mode | 1 | | 2 | | 3 | |
|---|---|---|---|---|---|---|
| Freq.(Hz) | 44.73 | | 82.12 | | 85.31 | |
| Damp(%) | 4.643 | | 2.203 | | 2.163 | |
| | Amp. | Phase | Amp. | Phase | Amp. | Phase |
| | 4.355e−01 | −0.11 | 1.946e−01 | 7.50 | 1.384e−01 | 174.25 |
| | 5.533e+02 | 0.00 | 4.232e+02 | −169.10 | 2.930e+02 | −7.20 |
| | 1.810e+00 | 124.90 | 4.744e+02 | 0.00 | 6.797e+02 | −0.00 |

| | Physical Matrices | | | Updated Matrices | | |
|---|---|---|---|---|---|---|
| | 6.03e−06 | −1.09e−10 | 2.55e−11 | 5.952e−06 | 6.278e−27 | 6.446e−27 |
| Mass | −1.09e−10 | 2.25e−12 | 6.63e−16 | −1.708e−25 | 2.176e−12 | −4.987e−29 |
| | 2.55e−11 | 6.63e−16 | 1.35e−12 | 1.608e−26 | −8.922e−29 | 1.361e−12 |
| | 9.25e+05 | −3.62e+02 | −1.64e+01 | 9.136e+05 | −3.389e+02 | −1.646e+01 |
| Stiff. | −3.62e+02 | 4.56e−01 | 1.52e−02 | −3.389e+02 | 4.305e−01 | 1.312e−02 |
| | −1.64e+01 | 1.52e−02 | 3.79e−01 | −1.646e+01 | 1.312e−02 | 3.828e−01 |
| | 2.772e−01 | −1.306e−04 | 1.064e−04 | 1.002e−01 | 1.181e−05 | −2.205e−05 |
| Damp. | −1.306e−04 | 1.816e−07 | −1.099e−07 | 1.181e−05 | 7.067e−08 | −9.755e−09 |
| | 1.064e−04 | −1.099e−07 | 3.320e−08 | −2.205e−05 | −9.755e−09 | 3.090e−08 |

c) Result table

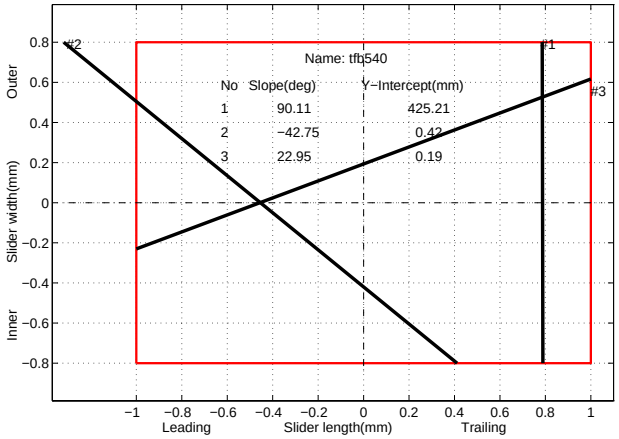


d) Nodal lines (14.14 m/s, 0 skew angle)

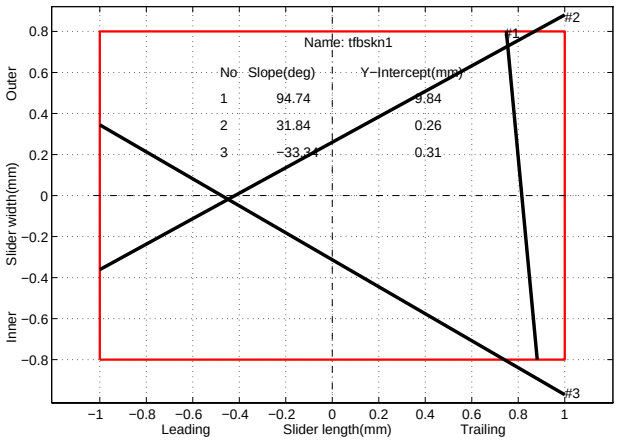


e) Nodal lines (14.14m/s, -10 skew angle)

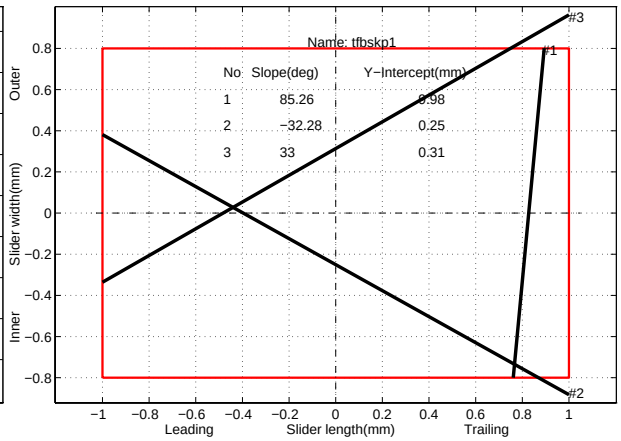


f) Nodal lines (14.14 m/s, 10 skew angle)

Figure 10 The Bow Tie shaped rail slider (TFB) and its results

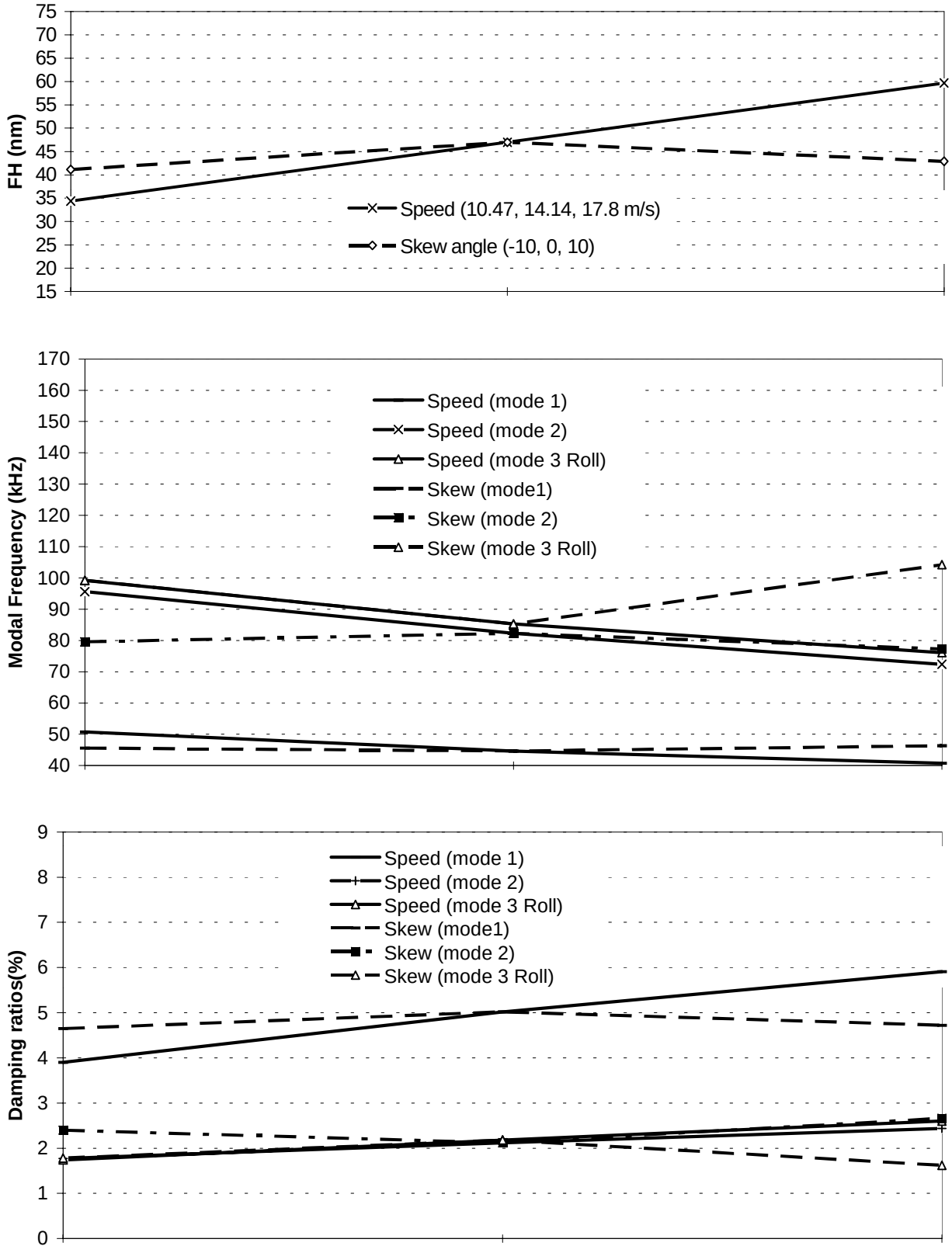


Figure 11 FH, Frequency and damping ratio vs the speed and skew angle of slider TFB

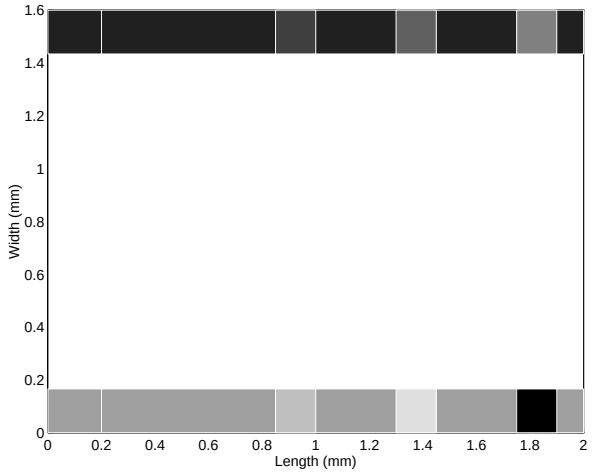


a) Rails

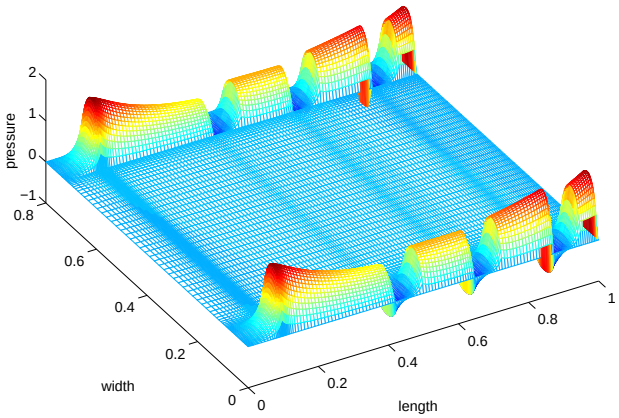


b) Pressure profile

Results Table

Name: td2 Flying height=47.53 nm

| Mode | 1 | | 2 | | 3 | |
|---|---|---|---|---|---|---|
| Freq.(Hz) | 47.25 | | 68.23 | | 86.23 | |
| Damp(%) | 5.035 | | 4.479 | | 3.39 | |
| | Amp. | Phase | Amp. | Phase | Amp. | Phase |
| | 3.782e−01 | 4.98 | 3.083e−01 | −179.35 | 2.448e−02 | 179.20 |
| | 6.304e+02 | 0.01 | 5.002e+02 | −0.00 | 3.460e+01 | −0.30 |
| | 6.241e+00 | 20.81 | 7.314e+01 | 177.70 | 8.183e+02 | −0.00 |

| | Physical Matrices | | | Updated Matrices | | |
|---|---|---|---|---|---|---|
| | 6.00e−06 | −1.15e−10 | 9.15e−12 | 5.952e−06 | −4.824e−26 | 0.000e+00 |
| Mass | −1.15e−10 | 2.21e−12 | −4.55e−15 | −3.887e−25 | 2.176e−12 | −7.959e−29 |
| | 9.15e−12 | −4.55e−15 | 1.37e−12 | 4.381e−26 | −7.647e−29 | 1.361e−12 |
| | 8.24e+05 | −1.92e+02 | −1.85e+01 | 8.188e+05 | −1.743e+02 | −2.041e+01 |
| Stiff. | −1.92e+02 | 3.04e−01 | 8.46e−03 | −1.743e+02 | 2.943e−01 | 7.664e−03 |
| | −1.85e+01 | 8.46e−03 | 4.01e−01 | −2.041e+01 | 7.664e−03 | 3.988e−01 |
| | 3.861e−01 | 1.714e−05 | 1.500e−06 | 2.937e−01 | −1.457e−05 | −8.786e−08 |
| Damp. | 1.714e−05 | 7.451e−08 | 1.760e−09 | −1.457e−05 | 4.154e−08 | 1.928e−09 |
| | 1.500e−06 | 1.760e−09 | 5.005e−08 | −8.786e−08 | 1.928e−09 | 4.982e−08 |

c) Result table

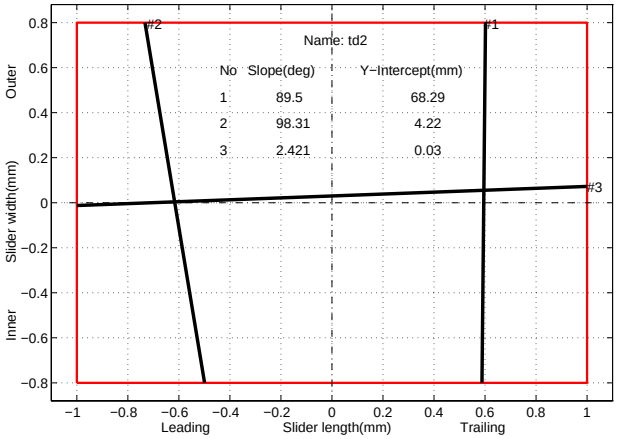


d) Nodal lines (14.14 m/s, 0 skew angle)

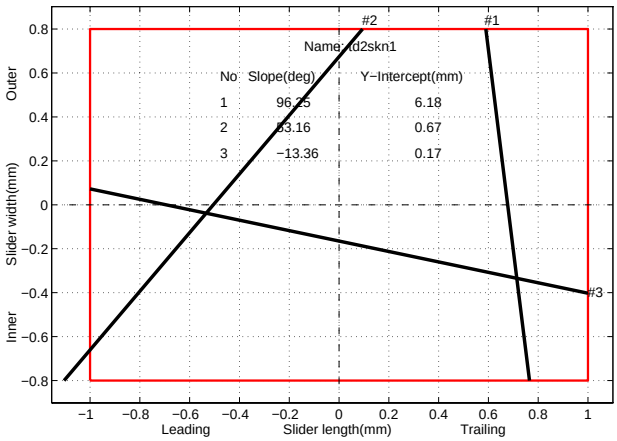


e) Nodal lines (14.14m/s, -10 skew angle)

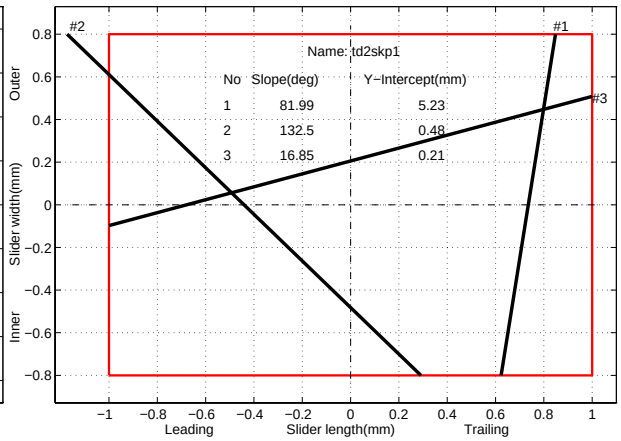


f) Nodal lines (14.14 m/s, 10 skew angle)

Figure 12 The transverse cut-off slider (TFT) and its results

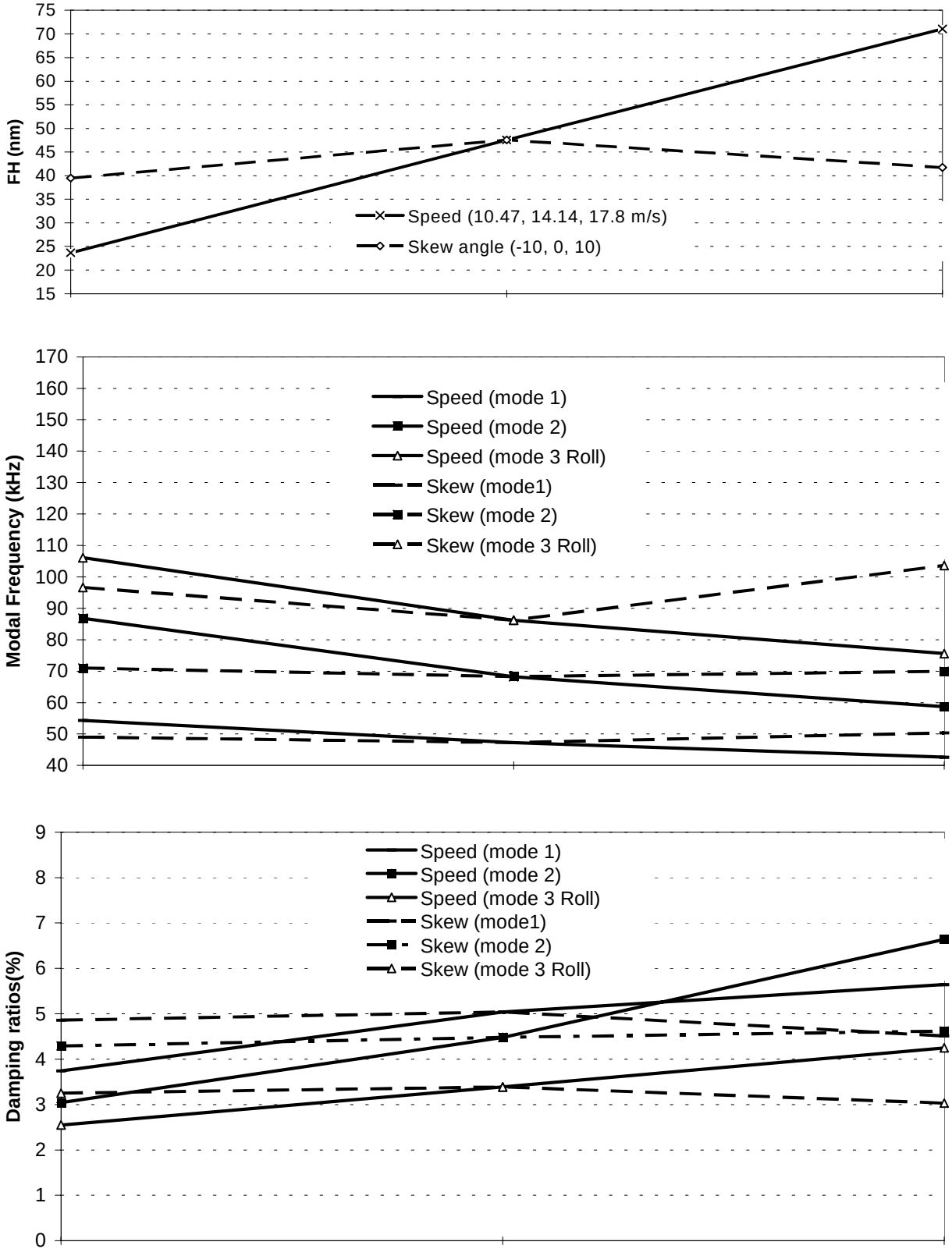


Figure 13 FH, Frequency and damping ratio vs the speed and skew angle of slider TFT

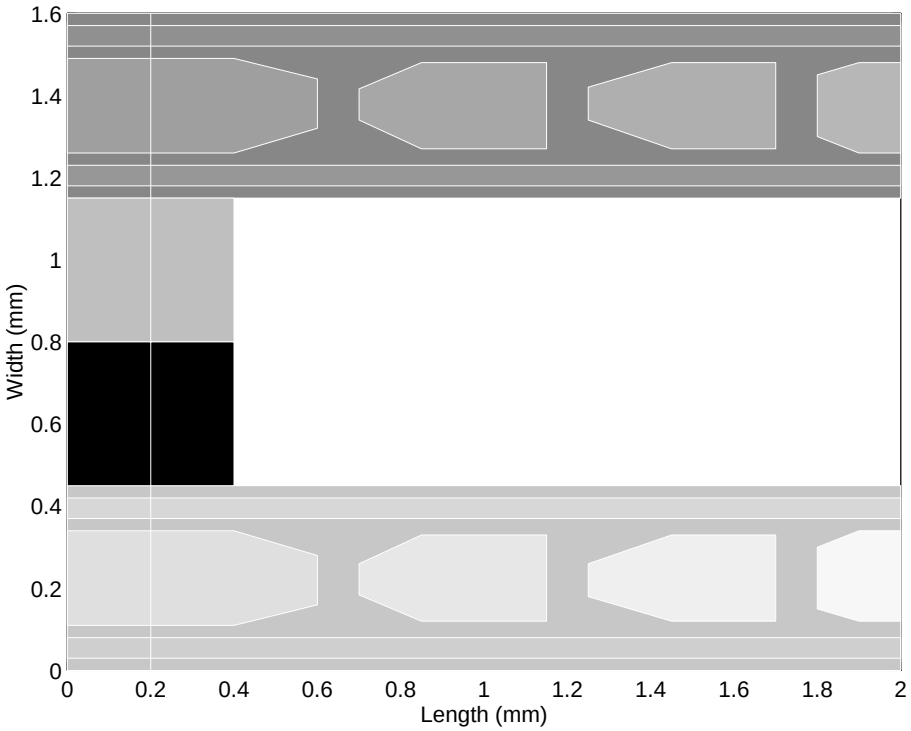


a) 2-D Rails

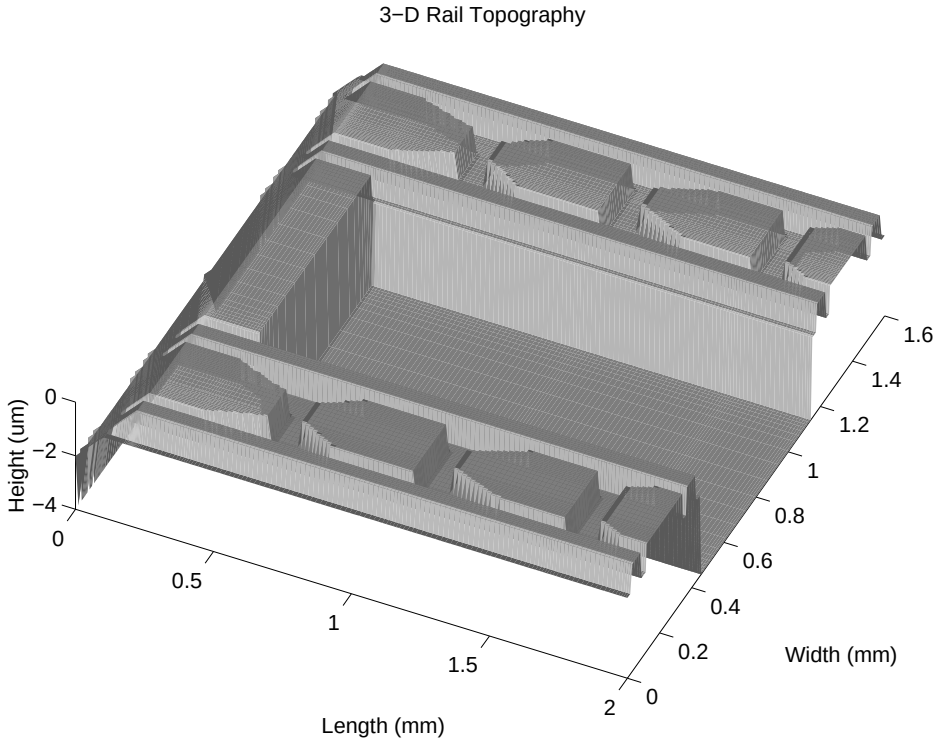


b) 3-D Rails

Figure 14 The HDS slider

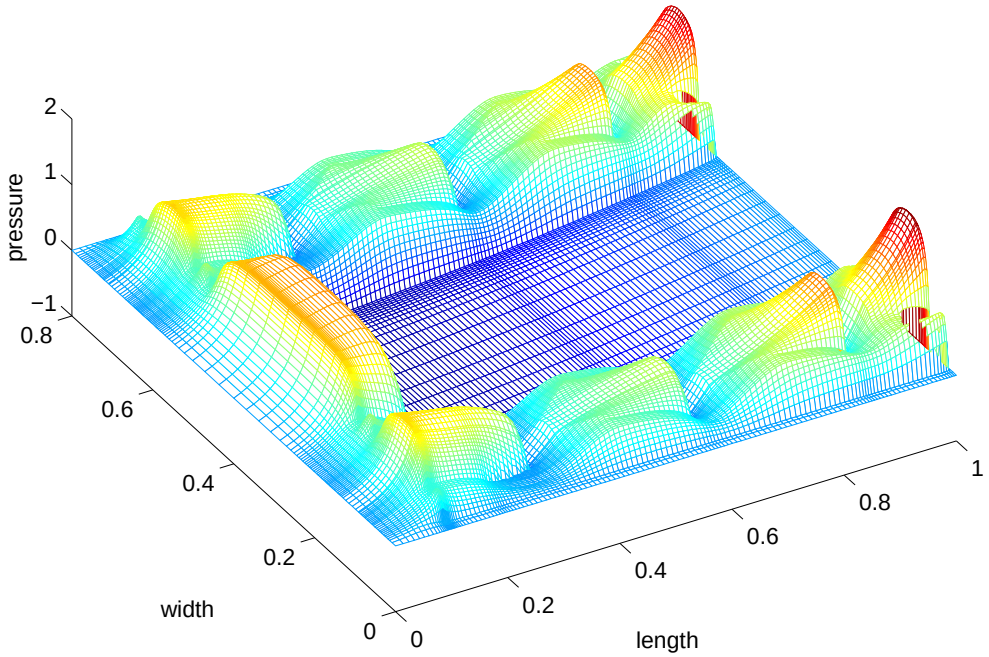


Figure 15 Pressure profile of the HDS slider

Results Table

Name: hds  Flying height=48.9 nm

| Mode | 1 | | 2 | | 3 | |
|---|---|---|---|---|---|---|
| Freq.(Hz) | 56.22 | | 82.27 | | 91.72 | |
| Damp(%) | 5.229 | | 5.19 | | 3.856 | |
| | Amp. | Phase | Amp. | Phase | Amp. | Phase |
| | 3.895e−01 | −1.26 | 5.006e−02 | 3.50 | 2.317e−01 | −178.59 |
| | 4.907e+02 | −0.00 | 1.143e+02 | −177.93 | 4.873e+02 | 0.00 |
| | 5.031e+00 | −4.43 | 8.175e+02 | −0.00 | 1.722e+02 | 2.84 |

| | Physical Matrices | | | Updated Matrices | | |
|---|---|---|---|---|---|---|
| | 5.83e−06 | 9.18e−12 | 1.83e−11 | 5.952e−06 | −6.613e−27 | −9.723e−27 |
| Mass | 9.18e−12 | 2.19e−12 | −5.65e−15 | 8.886e−26 | 2.176e−12 | 4.905e−28 |
| | 1.83e−11 | −5.65e−15 | 1.38e−12 | 1.047e−26 | 4.796e−28 | 1.361e−12 |
| | 1.17e+06 | −3.50e+02 | −2.08e+01 | 1.197e+06 | −3.552e+02 | −2.723e+01 |
| Stiff. | −3.50e+02 | 5.52e−01 | 1.56e−02 | −3.552e+02 | 5.496e−01 | 1.791e−02 |
| | −2.08e+01 | 1.56e−02 | 3.73e−01 | −2.723e+01 | 1.791e−02 | 3.682e−01 |
| | 2.408e−01 | −5.378e−05 | −1.291e−06 | 2.550e−01 | −1.643e−05 | 1.793e−06 |
| Damp. | −5.378e−05 | 9.386e−08 | −4.477e−10 | −1.643e−05 | 8.473e−08 | −3.195e−09 |
| | −1.291e−06 | −4.477e−10 | 7.719e−08 | 1.793e−06 | −3.195e−09 | 7.252e−08 |

Figure 16  Result table of the HDS slider

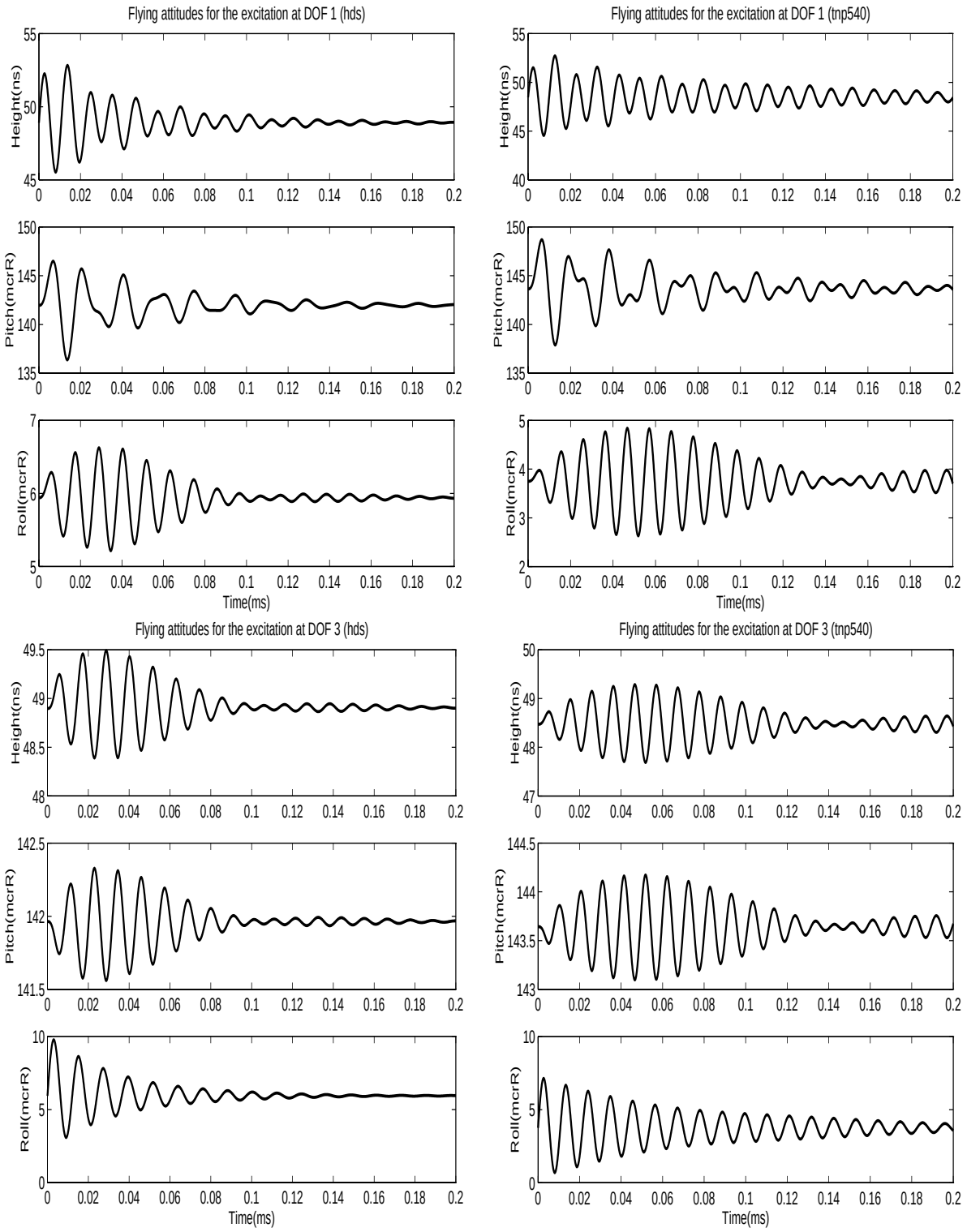


a) The HDS slider b) The TNP slider

Figure 17 The dynamic responses for the impulse excitations in the vertical and roll directions

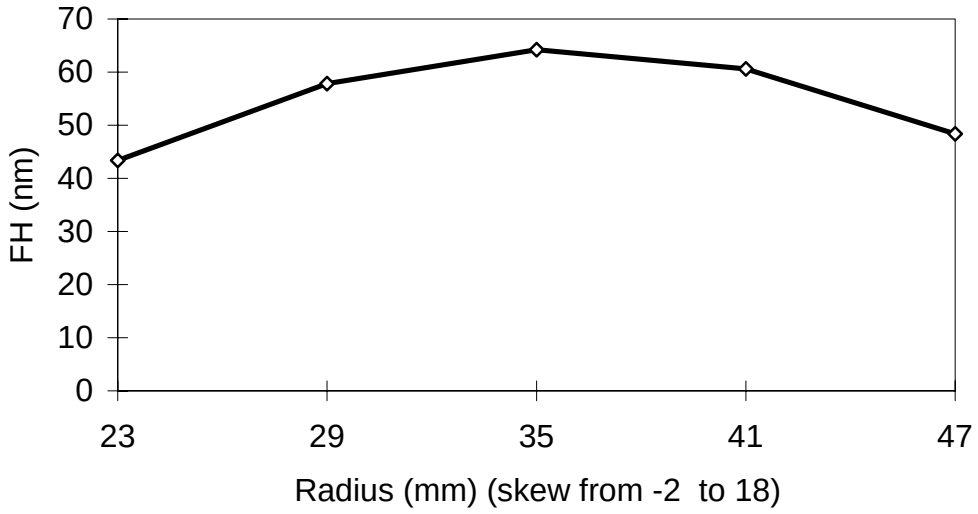


Figure 18 The FH profile of the HDS slider